Development of a Shock Table Using Finite Element Analysis

Mafalda Santos

Delft University of Technology

TU Delft

Development of a Shock Table Using Finite Element Analysis

by

Mafalda Santos

Mafalda
Santos

Instructor:	I. Uriol Balbin
UARX Space Advisor:	F. Larco
Project Duration:	January 2024 - March, 2025
Faculty:	Faculty of Aerospace Engineering, Delft

Cover:	Starlink Group 7-17 | Falcon 9 Block 5 lift-off by SpaceX and Jack Beyer
Style:	TU Delft Report Style, with modifications by Daan Zwaneveld

TU Delft

Contents

Nomenclature

Abbreviations

Abbreviation	Definition
AHP	Analytic Hierarchy Process
CAD	Computer Aided-Design
CBUSH	Generalized Spring and Damper Structural Element
ESA	European Space Agency
FEA	Finite Element Analysis
FEM	Finite Element Method
FRF	Frequency Response Function
GA	Genetic Algorithms
MDOF	Multi Degree of Freedom
MIPS	Mechanical Impulse Pyro Shock
MPE	Maximum Predicted Environment
NASA	National Aeronautics and Space Administration
RBE	Rigid Body Element
SDA	Statistical Energy Analysis
SDOF	Single-degree-of-freedom
SEM	Spectral Element Method
SRS	Shock Response Spectrum
STF	Shock Test Facility

Symbols

Symbol	Definition	Unit
c	damping coefficient	[-]
E	Energy	[J]
$F(t)$	applied force, derived from the input acceleration	[N]
g	gravitational acceleration	[-]
h	height	[m]
k	stiffness	[-]
m	mass	[kg]
v	Velocity	[m/s]
w_{max}	Maximum frequency	[Hz]
x	displacement	[m]
$\dot{x}$	velocity	[m/s]
$\ddot{x}$	acceleration	$[m/s^2]$
δ_t	Time step	[s]

1

Introduction

Throughout their lifetime, spacecraft have to survive harsh environmental conditions that require robust design and testing to ensure their survival. As such, before they are cleared for launch, they must pass rigorous testing, including a shock test that stands out as a critical assessment to ensure structural integrity under extreme mechanical loading conditions. In a mission, a spacecraft can be exposed to shock due to an impact or explosion, which can be caused during launch and separation fairing or due to the deployment of appendages, for example [1].

Shock is a local transient mechanical load characterised by its short duration, high frequency, and high amplitude [2]. It can be conceptualised as a non-periodic excitation of a mechanical system, caused by sudden and significant accelerations or displacements to system components.

Shock propagation involves intricate wave phenomena, including reflection, dissipation, and diffraction at boundary conditions or mechanical discontinuities, such as a hole, or joint [3]. The propagation of shock waves is also affected by damping and attenuation mechanisms, specially at high frequencies, which leads to a rapid dissipation of energy over time and space [2]. Therefore, the response of a system to shock excitation is highly oscillatory, with high acceleration peaks, both positive and negative, typically returning to zero within milliseconds. Since the excitation times are significantly shorter than the response times of the system, the system is allowed to respond freely to the imposed mechanical loading [3].

The impact of shock on mechanical system can be profound, with the potential to cause major damage on a spacecraft and its equipment. The impact severity may vary depending on factors such as shock magnitude, duration, and system structure. Nonetheless, the consequences can be significant, ranging from functional incapacitation to catastrophic failures. In fact, mission failure has occurred more often due to shock than due to vibration, likely because the understanding of shock is more limited [4].

Since the energy transmitted by shock events contains mostly high frequency content, which typically does not harm structural members, often the most affected areas of the spacecraft are electronics, mechanisms and valves [2].

Shock can have various characteristics, including magnitude, duration, frequency, waveform, and directionality. These characteristics affect how a structure will behave when subjected to the shock load. For instance, the magnitude of the shock determines the force exerted into the structure, while the duration influences the material's response. The waveform can range from simple pulses to complex waveforms, and its frequency affects the resonance and vibration behaviour. Lastly, shock loading can be unidirectional, occurring along a single axis, or multi-directional, occurring along multiple axes simultaneously [4]. The directionality of the shock load can affect how materials and structures respond to the impact.

Due to the diverse nature of these characteristics and their implications for structural integrity, it is essential to categorise shock loading, as it helps in understanding and addressing the unique challenges posed by different types of shock.

When the shock is characterised by a sudden and violent change in the net velocity of the system, it is called a velocity shock [4]. This type of shock typically occurs over a short duration compared to the periods of the main natural frequency of the system, inducing a significant amount of energy levels around it, which can lead to structural damage [3]. A displacement shock occurs when the net velocity change is zero, due to two or more velocity shocks with equal and opposite velocity magnitudes [4].

High frequency shocks are high acceleration and high frequency oscillations that also result in a net velocity of zero [4]. These shocks are quickly dampened, and while they don't usually excite the principal natural frequencies of the system, they still pose a threat to the system, particularly for electronics and brittle materials [3].

Pyroshocks, which will be the focus of this project, are high frequency shocks commonly observed in aerospace vehicles. These shocks are usually caused by pyrotechnic devices and, due to distance and number of discontinuities to the source, are quickly dampened [4]. A pyroshock environment depends on multiple parameters such as the type of source, the geometry and properties of the structure, and the distance [4]. However, there are no rules that define a shock through its distance to the source and so the following distinction is made:

The near-field, which is close to the pyrotechnic source, is characterised by direct wave propagation that causes high peak accelerations and high frequency content [2]. In fact, the acceleration levels can exceed 10000g, and the frequency content may extend well beyond 10 kHz [1]. The mid-field environment combines the direct propagation of waves with structural resonances. Thus, it exhibits lower acceleration peaks, ranging from 1000g to 10000g, and a less wide frequency range, only up to 10 kHz [2]. The far-field environment is dominated by structural resonance, leading to much lower peak accelerations, typically below 1000g, and the frequency content is concentrated below 10 kHz [2]. Nonetheless, despite the greater distance from the source and the lower acceleration peaks, the severity of the far-field environment may not necessarily decrease, especially when high structural resonances dominate the frequency range [2].

Shock is a complex phenomenon, which makes it virtually impossible to exactly replicate shock conditions that occur on the field in the time domain. As such, the Shock Response Spectrum (SRS) is commonly used in the aerospace industry to assess the potential damage and to describe test specifications. The SRS is determined by applying the acceleration time history of a shock to a standardised array of single-degree-of freedom (SDOF) systems and determining the maximum responses [4]. This calculation is not bijective, which means that, if given a Shock Response Spectrum curve, it is not possible to obtain the original acceleration time history of the structure due to loss of important information throughout the process.

This method provides a way of comparing shocks, as the shock effect is described on a standardised dynamical system, as different shock waveform can give the same SRS. As such, SRS is often used as a test specification because different test setups generate similar SRS [2].

Moreover, SRS curves exhibit characteristic shapes that provide additional insight into the shock event. For instance, when the net velocity change is zero, which is the point of interest in this study, the SRS follows a distinct pattern: an initial slope typically ranging from 6 to 12 dB per octave, a steady increase until the knee frequency, and a subsequent plateau [2]. The knee frequency marks the transition point between the rising portion of the curve and the flat plateau. These features help define the expected behaviour of a system and serve as a reference for evaluating test results.

To recreate an SRS curve, a lot of trial and error is required [3]. The key parameters identified to tune it to the desired levels are the resonant fixture shape, material, dimensions and boundary conditions, the impact velocity, impactor material, shape and mass, anvil material, impact location and measurement.

As previously mentioned, SRS is often used as a specification for testing, but the test levels depend on what kind of testing is being made. The SRS levels are obtained through the maximum predicted environment (MPE), which can be estimated through analytical models, direct measurements, and extrapolation methods from previous measurements.

For qualification testing, the goal is to prove that a hardware's design and manufacturing process result in equipment that fulfils the environmental requirements [3]. The specimen used for testing is not flight

hardware but the qualification model and has to survive the testing with appropriate margins. To qualify it, a margin of at least 3 dB is added to the MPE [5].

The acceptance test has the goal of demonstrating that the flight hardware is representative of the qualified equipment, meaning it is free of workmanship errors and material defects [3]. These tests have a short duration and lower test levels than qualification tests to avoid overtesting it.

However, space equipment is often unique and only one is built, which means that these tests are combined into a protoflight test [3]. These tests are shorter and have lower levels to avoid wearing out the hardware [6].

Once the test levels are determined, the SRS is calculated using constant slopes that can be recreated in shock testing. On top of this level, tolerances are applied to allow for the STF to have some margin to work.

However, these margins are not universal, and different organisations apply different tolerances. For example, ESA applies a -3 dB/ +6 dB margin where at least 50% of the SRS amplitude has to be above 0 dB, whereas NASA applies a $\pm$6 dB up to 3000 Hz and -6 dB/ +9 dB above that [6][7].

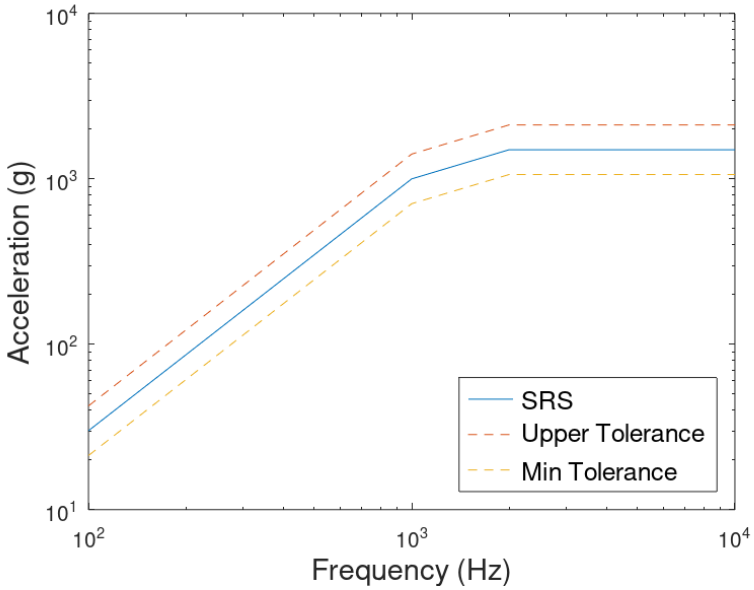

Figure 1.1: Required SRS levels with tolerances [7].[6]

As such, shock testing facilities must be meticulously designed to replicate the required shock levels within these tight tolerances. Due to the complexity of shock events, including their high frequencies, durations, and magnitudes, achieving precise reproduction in a laboratory setting is particularly challenging [2]. As a result, testing equipment must be carefully engineered to ensure that these specifications are met consistently and reliably.

To address these challenges, the goal of this project is to understand how useful finite element analysis (FEA) is in the development of a shock table capable of testing heavy equipment to the required Shock Response Spectrum (SRS) levels, as illustrated in Figure 1.1. The primary objective is to assess the accuracy of FEA in predicting shock behaviour and to understand how different modelling approaches, solution methods, and levels of detail in the models impact both accuracy and computational cost.

In particular, the study will examine the trade-offs between highly detailed, computationally expensive models and simpler, faster ones that may compromise on accuracy. As such, various modelling strategies will be explored, including the use of different element types to represent components of the system, as well as assessing the impact of including or omitting certain components altogether. The influence of mesh density and time step size will also be investigated to evaluate their effect on computational cost and solution accuracy.

Furthermore, two different solution approaches, Direct Transient Analysis and non-linear implicit transient analysis, will be compared in terms of accuracy and computational efficiency. This comparison aims to clarify the compromises involved in selecting either method and to identify the contexts in which each may be most appropriate.

Additionally, the study will investigate how FEA can predict the impact of various design parameters—such as fixture shapes, material properties, and boundary conditions—on the resulting SRS. By better understanding these factors, this research aims to optimise the design process of shock testing equipment, ensuring it meets the demanding requirements for effective testing.

1.1. Literature Review

Despite advancements in shock testing methodologies, challenges persist in accurately predicting and validating spacecraft behaviour under diverse shock scenarios. This literature review focuses on two key areas within the shock testing field that are particularly relevant to the project.

The first area involves the investigation of experimental shock test facilities will provide valuable insights into the current state of the art, methodologies, techniques, and designs that can guide the development of the shock table. As such, understanding the capabilities and limitations of existing experimental facilities is essential for designing an effective shock test setup.

The second area of study focuses on simulation methodologies. Given the project's objective to model a shock table using finite element methods (FEM), exploring simulation techniques is crucial. By examining the current state of the art research in simulation, this literature review aims to assess the feasibility and accuracy of using FEM and other methodologies to replicate shock.

By delving into both experimental and simulation studies, this literature review seeks to provide a comprehensive understanding of the current landscape in shock research, offering valuable insights for the development and validation of shock testing methodologies.

1.1.1. Shock Test Facilities

Shock testing is a critical aspect of spacecraft design, with many studies focusing on the development of testing apparatus and verification protocols. These facilities aim to recreate shock environments to which equipment is subjected during operational conditions. There are several methods to experimentally recreate these shock environments, each with its own advantages and limitations.

One approach is to use live ordnance with the actual system structure [8]. This method is capable of producing an almost identical shock environment, but can also be very expensive and damaging to the structures. As such, it is common to use other methods for testing, with various methods for excitation. Depending on the shock environment that is intended to be recreated, the shock test facilities (STF) will have different characteristics, with different methods of excitation.

Far-field STFs are designed to replicate shock environments that occur at a distance from the source of the shock, typically featuring lower peak acceleration levels and narrower frequency bands as previously mentioned. These facilities are then commonly used to simulate shock conditions at lower intensities, where higher operational costs or risks associated with more destructive methods are not justified.

Shakers can not only be used for vibration testing, but also as a shock testing facility for far-field shock environments. They are are versatile testing devices capable of generating controlled vibrations across a wide frequency range, and as such are often used due to their low operational cost and high availability. However, it's important to note that shakers have limitations when performing shock tests, as they can not recreate excitation above 3000 Hz and 300 g [2].

Another method employed in far-field STFs is the use of drop tables. Drop tables provide a means of subjecting test items to controlled impacts or shocks by dropping them from a specified height onto an anvil [2]. However, drop tables can only be utilised in very specific applications as they often result in over-testing at low frequencies due to the high net velocity change and energy levels they produce, which makes them unsuitable for high-frequency shocks [4].

Mid-field shock testing facilities replicate shock environments that occur at intermediate distances from

the source. These facilities typically involve subjecting test items to mechanical impact by attaching them to resonant fixtures. Therefore, mid-field STF usually comprehend of two main parts: the resonant fixture and the impactor. Both the impactor and resonator used vary significantly, from handheld hammers to air guns, and from resonant plates to bars and beams, respectively [4].

The resonance fixtures are used to induce resonance into the test specimen, as they are designed to have their dominant frequencies match the knee frequency of the desired SRS, minimising iterative tuning efforts. Additionally, they are designed to be robust, with substantial thickness and mass compared to the structures under test, in order to avoid external influences and produce repeatable results [4]. The use of thick resonant fixtures is also beneficial due to their adaptability, as different test items can be attached without significantly affecting the fixture's response which makes them useful in a wide range of applications.

Resonant plates usually consist of rectangular plates suspended freely, often supported by foam padding or bungee cords. The specimen being tested is generally attached near the centre of the plate, which is then excited by a mechanical impact. They are designed to ensure that the first bending mode matches the knee frequency of the test requirement.

A resonant bar is also freely suspended, often featuring a rectangular cross-section where the test item is attached at one end of the bar while on the opposite the impact occurs [4], as shown in Figure 1.2. For resonant bars, the first longitudinal mode should be aligned with the desired knee frequency, meaning the length of the bar is the main design driver of this type of resonant fixtures. The other dimensions of the bar can be adjusted to accommodate the test item, as long as they remain significantly smaller than its length.

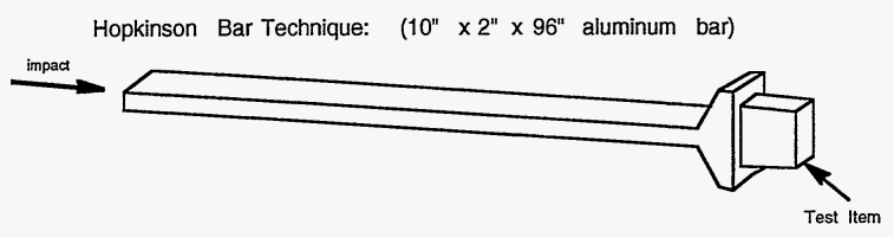

Figure 1.2: Shock Facility with a bar as resonant Fixture [8]

Even though designing a resonant fixture with a specific knee frequency aligned with test specifications requires less fine-tuning of the test setup, it means that different resonant fixtures are required for different test requirements [8]. To avoid having a large inventory of resonant fixtures, tunable resonant fixture methods have been developed, which allow for the adjustment of the knee frequency for a single test apparatus.

For example, for the resonant bar previously described, it is possible to adjust the knee frequency by attaching weights to specific locations along the length of the bar that correspond to different modes of vibration [9]. This would enable the testing of various shock spectrum curves without needing an inventory of multiple resonant fixtures.

To provide the mechanical impact required for resonant testing, various methods can be employed, including the use of pendulum hammers, pneumatically driven pistons, and air guns [4]. These methods offer repeatability and control over impact force magnitude and duration, essential factors in achieving consistent and accurate test results.

To recreate near-field shock environment it is common to attach the specimen to a resonant plate which is then excited with explosives, as shown in Figure 1.3. However, even though it is quite difficult due to the characteristics and intensity of the shocks, there also exist STF that recreate near-field shock environments through mechanical impact [4].

In the aerospace industry, numerous shock testing facilities exist, each with unique designs and methodologies for simulating shock environments. While many of these facilities utilize the methods described earlier, others incorporate alternative techniques and approaches.

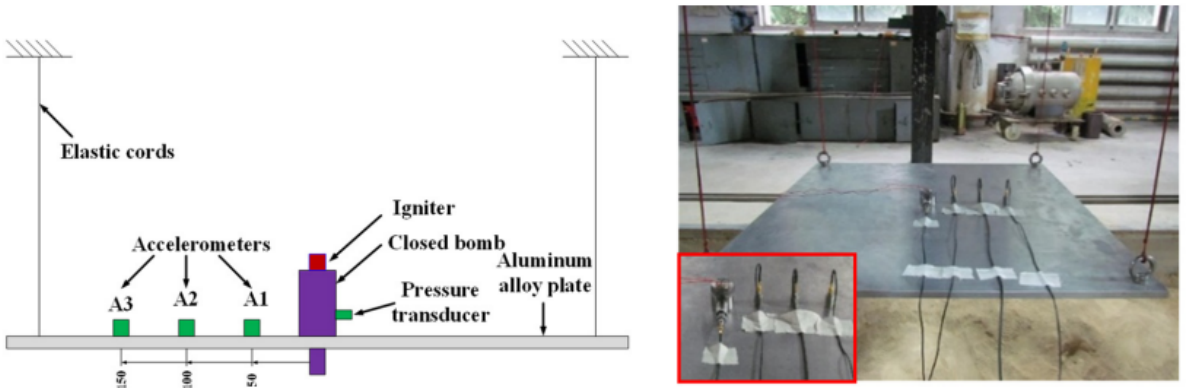

Figure 1.3: Shock Test Facility using explosives. Test setup (left) and shock table (right) [10]

NASA's Mechanical Impulse Pyro Shock (MIPS) Simulator is a facility capable of testing equipment up to 10000 g and weighing up to 23kg [11]. This STF consists of a 7075-T6 aluminium plate measuring 1.22m x 1.83m x 0.013m, which rests on a 7.6cm thick foam pad for damping, ensuring free boundary conditions for the resonant plate, as shown in Figure 1.4. The impact is generated by a pneumatic actuator, which leads to the resonance of the plate.

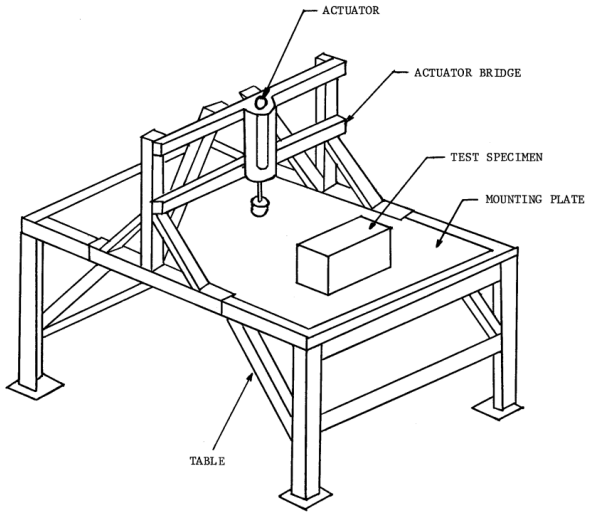

Figure 1.4: NASA MIPS [11].

The Dornier Shock Table features a horizontal aluminium plate mounted on a frame, which serves as the testing platform, seen in Figure 1.5. To induce shock, an impacting mass is dropped through a tube onto the plate. By using various impact masses and drop heights, it is possible to adjust the shock facility to enable a wide range of test requirements [12]. It has the capacity to test specimens of up to 30 kg and it has successfully tested equipment with dimensions up to 540x520x180mm.

The shock table developed by Martin Jonsson for space equipment qualification features an aluminium plate, with 1 x 1 x 0,03 m, set horizontally on a table over foam padding, shown in Figure 1.6. It uses a pendulum hammer dropped from various heights to excite the plate. This apparatus allows for the plate to be impacted in both the out-of-plane and in-plane direction by adjusting the position of the pendulum hammer, allowing for testing in different axis. Similarly, D. Risner developed a shock table for Cal Poly where a pendulum hammer excites an aluminium plate, with 1,22m x 1,83m, suspended vertically by cords [1].

One of the main issues encountered in these two designs was the inability to adjust the SRS levels for shocks in the in-plane direction. As such, Abdulla Almesmari et. al developed a STF with a similar design to Martin Jonsson's to try and address this issue. The solution found was to introduce a rubber

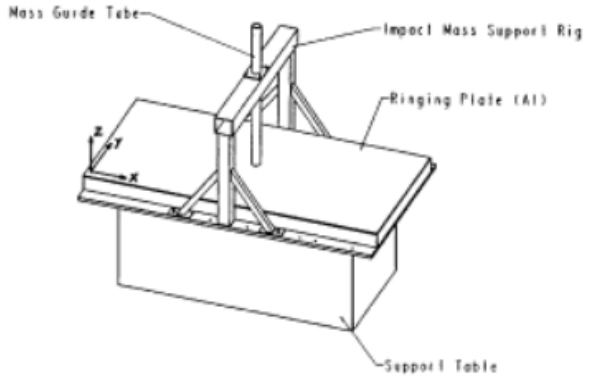

Figure 1.5: Dornier Table [12].

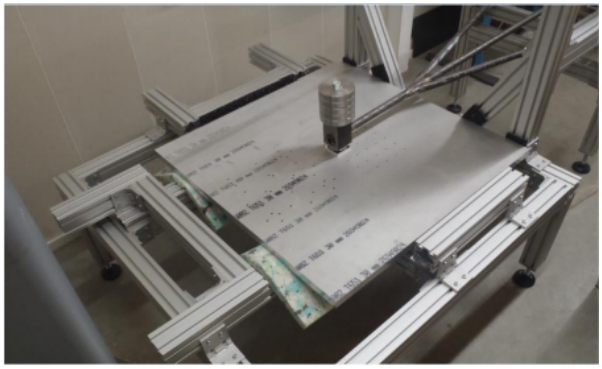

Figure 1.6: Shock Table With Resonant Plate and Pendulum Hammer [3].

pad that can amplify the shock levels as long as the the natural frequency of the dampening material is lower than the natural frequency of the testing equipment [13].

At Sandia National Laboratories, an apparatus has been developed which is capable of accommodating a 50x50 cm mounting base and adjusting the knee frequency between 500Hz and 3000Hz. This facility consists of a bar with fixed length where a variable quantity of mass is attached to the impact end, seen in Figure 1.7. By adjusting the mass, the resonant frequency could be altered between two extremes, allowing for a range of knee frequencies [8].

In another innovative design, So-Jeong Lee et al. employed a high-pressure air release device to accelerate a lightweight projectile, which impacts a resonant fixture. The fixture is compact and cylindrical in design to minimize the size of the apparatus [14]. Similarly, Ju-Won Jeong et al. used a pneumatic release device to strike a bar-type resonator attached to a resonant plate. This system allows the shock levels to be adjusted without modifying the resonance plate, simply by altering the length of the

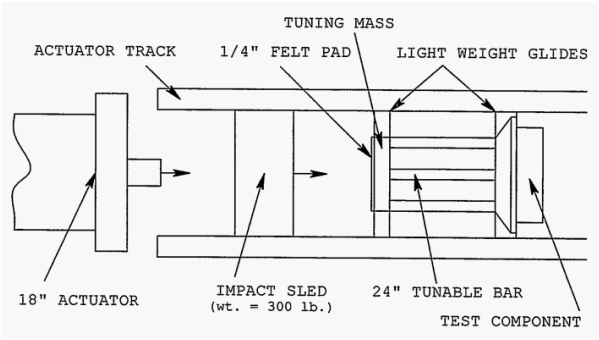

Figure 1.7: Set up of Shock Facility with a Tunable Resonant Bar. [8]

resonator [14].

Lastly, the shock table facility developed by Jae-Kyeong Jang et al. uses a laser-induced shock methodology to simulate pyroshock environments non-destructively. The system involves the generation of high-intensity laser pulses that interact with a target surface, inducing a rapid shock wave mimicking the effects of a pyroshock event [15]. The laser shock generation process is highly controlled, allowing precise tuning of shock characteristics such as amplitude and duration. The setup includes a laser system positioned to focus on the target material, a shock table to isolate the system from external vibrations, and sensors to measure the response, as seen in Figure 1.8.

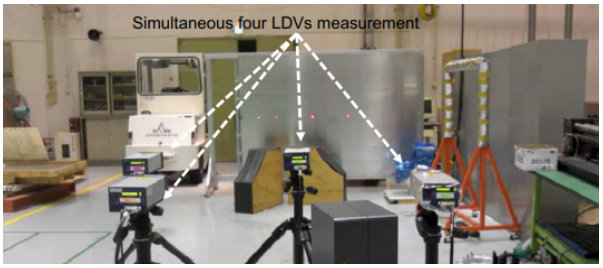

Figure 1.8: Laser-Induced Shock Table Facility [15].

This research review provides valuable insights into the experimental aspects of shock testing, focusing on the development of testing apparatus. By examining various methods for recreating shock environments, including live ordnance and mechanical impacts, this review offers a comprehensive understanding of the state-of-the-art techniques and their applications.

As such, this information will serve as a guide for the project's development of a shock table by summarising different shock test facility (STF) designs and methodologies. Understanding the characteristics and capabilities of existing STFs, such as far-field, mid-field, and near-field facilities, facilitates the decision-making process of selecting suitable components and design parameters for the project. Additionally, insights into the advantages and limitations of different resonant fixtures and impactors will have a significant impact on the design and optimization of the shock table.

1.1.2. Numerical Simulation

In addition to experimental studies, another key area of research focuses on the accuracy of predictive models, particularly Finite Element Models (FEM) and analysis techniques. While significant advancements have been made, further contributions are still needed in this field to improve the fidelity and efficiency of simulations.

Numerical analysis of shock behaviour is not as straightforward as the analysis of other load types, as it presents its own unique challenges. These challenges arise from the characteristics of shock loading like its short duration, the broad range of excitation frequencies, nonlinearity, and wave propagation effects [16].

The short duration of shock events demands the use of very small time steps in the analysis, leading to significantly longer computational times. This requirement arises from the need to accurately capture the rapid changes in loading conditions that occur during the brief duration of shock events. Consequently, computational resources and time become major considerations in conducting numerical simulations of shock behaviour.

Additionally, the broad range of excitation frequencies of shock loading poses further computational challenges. Effectively capturing such a broad frequency range requires sophisticated numerical techniques and algorithms capable of accurately resolving the dynamic response across multiple frequency domains. Furthermore, some numerical methods are more suited for lower frequencies while others provide more accurate results for higher frequencies [16].

Its non-linear behaviour also introduces complexities into the analysis process. Non-linearities can arise from material properties, contact interactions, and structural deformations under extreme loading conditions. Accounting for these non-linear effects requires advanced numerical models and solution

methods capable of accurately capturing the non-linear response of structures subjected to shock loading.

Finally, wave propagation effects present another significant challenge in shock analysis. As shock waves propagate through a structure, they interact with material interfaces, boundaries, and discontinuities, leading to complex wave interactions and reflections [16]. Capturing these wave propagation phenomena accurately is essential for predicting the dynamic response of structures to shock loading and requires sophisticated numerical techniques that account for wave propagation effects in the analysis.

Consequently, there is a variety of methods that have been developed to predict the behaviour of a system under shock loading. These numerical methods generally fall either into the implicit or explicit category. For implicit methods, the solution depends on both the current and future time steps. This involves solving a system of equations making it computationally more expensive, but with the upside of it being stable. On the other hand, explicit methods calculate the solution for the next time step solely based on the current time step, meaning they can be less computationally expensive. However, these methods are conditionally stable, which means that the time steps used have to be very small to satisfy Equation 1.1 and ensure stability. Therefore, explicit methods can have an advantage over implicit methods when the simulated phenomenon has a short duration, since small time steps are already needed.

$$\delta t \leq \frac{2}{w_{max}}, \tag{1.1}$$

where δt represents the time step, and w_{max} is the maximum frequency present in the system.

Among numerical methods, finite element analysis (FEA) stands out as one of the most widely used approaches, due to its wide availability and use for other types of loading in many engineering industries. Within FEA, there are various methods that can be applied in order to perform a shock analysis. The work of Andrés García-Pérez et al., as presented in "Overview and application of FEM methods for shock analysis in space instruments," provides valuable insights into the application of FEM methods for shock analysis, such as transient analysis, Response Spectrum Analysis (RSA), Sine Transmissibility method and Equivalent Quasi-Static Load Method [16].

Transient analysis evaluates how a structure responds to loads that change over time, generating results as time-dependent functions. The SRS curves and the peak values can then be easily calculated with the results obtained in the time functions. Therefore, the behaviour of the system under analysis can be completely obtained, at the cost of increased computational time.

Transient Analysis simulates the behaviour of structures subjected to time-varying loads, generating detailed time-dependent results. This approach offers a detailed view of how the system behaves under dynamic loading by capturing its response over time — including peak values, time-dependent data, and the progression of the response [16]. The SRS curves and the peak values can then be easily calculated with the results obtained in the time functions. Therefore, Transient Analysis is especially useful when the structure is subject to complex, time-dependent loads that require detailed analysis, such as shock waves or impact events, at the cost of increased computational time.

Response Spectrum Analysis (RSA) estimates the maximum structural response by evaluating each vibration mode and then combining these contributions into a total response estimate. This technique is especially valuable for evaluating the effects of dynamic loading, such as shocks or vibrations, without the need to compute the full time-domain response. Its main advantage is its computational speed; however, its accuracy depends on the mode combination method used and may decrease when applied to highly non-linear or complex systems. It is most effective in scenarios where detailed time-dependent behaviour is not critical or when a rapid approximation of peak response is sufficient [16].

The SRS curves in the Sine Transmissibility Method are obtained by scaling the input SRS with the transmissibility function between the base and the target nodes. This method is beneficial for situations where the response acceleration to a sinusoidal shock can be approximated based on the transmissibility characteristics of the system. However, while it provides insight into the dynamic amplification of forces, it does not provide full time-dependent results such as peak values or detailed time histories.

This method is most useful in situations where the shock is relatively simple or sinusoidal in nature, but it is limited in cases involving complex or transient shock events that require more detailed analysis [16].

Finally, the Equivalent Quasi-Static Load Method simplifies shock load analysis by approximating the dynamic shock load as a static force based on the inertial acceleration experienced by the structure. Instead of modelling the time-varying shock load in full detail, this method assumes that the peak shock effect can be represented by a static load equivalent to the maximum inertial force the structure experiences. This method essentially replaces the complex dynamic response with a simpler static approximation, significantly reducing computational requirements. However, it only captures the inertial effects of the shock and does not account for other dynamic behaviours, such as vibrations or resonances, that may be important in certain scenarios [16].

FEA methods serve a wide range of purposes in predicting shock behaviour and can provide valuable insights into equipment design and performance under shock conditions. For example, Bae-Seong Kim et al. utilised FEA to design a pyroshock testing device, optimising the shape of a conical resonator to generate the desired SRS [17].

"In a separate study, Tuncay Yalçinkaya et al. combined finite element analysis (FEA) with experimental observations to obtain the Shock Response Spectrum (SRS), allowing a direct comparison between test outcomes and simulation results for real equipment behaviour [18]. This approach improves the accuracy of the results and increases the reliability of the simulations.

FEA's applicability extends beyond structural components to other areas as well. For instance, Xixiong Wang et al. applied FEA to predict the behaviour of separation nuts subjected to shock environments, demonstrating its utility in analysing mechanical components [19]. Furthermore, Dattatraya R. Hipparkar et al. utilised FEA to characterise the acceleration pulse of Neoprene rubber used as a pulse-shaping material, further illustrating FEA's versatility in shock testing applications [20].

In addition to FEA, other methods such as Statistical Energy Analysis (SEA), Spectral Element Method (SEM), and Hydrocodes have been developed to simulate shock phenomena [16]. Hydrocodes, in particular, have been an area of active research due to their potential to offer more accurate results at a reduced computational cost.

For instance, in a study conducted by Luca Viale et al., a hydrocode was utilised to numerically model a resonant plate for shock testing [21]. The study focused on capturing the transverse dynamic response of rectangular plates with varying geometries using a Multi-Degree-of-Freedom (MDOF) modelling approach. It allowed for the definition of geometric parameters such as base, height, and thickness, which affect mass. The study proposed a method for tuning each test using matrices of stiffness, damping, and mass. The results showed that the numerical method could be used for the design, dimensioning, and tuning of the plate.

To enhance the precision of their findings, the researchers developed a more sophisticated numerical model tailored to optical and electronic systems commonly found in space missions, which are particularly vulnerable to shocks and high-frequency vibrations [22]. Using a Frequency Response Function (FRF) method, the study determined the resonant plate's dynamic behaviour, integrating a Computer-Aided Design (CAD) tool with a finite element solver. The investigation covered key factors such as impulse characteristics, geometric complexity, and force profile acquisition. The findings demonstrated that the proposed approach effectively captured shock responses and offered valuable guidance for optimising system design through Genetic Algorithms (GA).

This literature review has examined the challenges and advancements in utilizing Finite Element Analysis (FEA) for simulating shock environments, particularly within the context of shock table testing. The review has highlighted key obstacles, such as the non-linearities inherent in material and structural responses, the necessity for small time steps to accurately capture the transient nature of shock loading, and the complexities associated with wave propagation effects. These factors underscore the importance of careful modelling and the need for precise simulation strategies to reliably predict Shock Response Spectrum (SRS) levels.

The various FEM techniques reviewed, including transient analysis and response spectrum methods, offer valuable insights but also present limitations, particularly in terms of computational efficiency and

the accuracy of the results. Additionally, the impact of parameters such as mesh size, element type, and time step on simulation accuracy is significant, emphasizing the necessity to address these factors when conducting shock testing simulations.

In this context, the central focus of this thesis is to assess the accuracy with which Finite Element Models (FEM) and analysis can predict Shock Response Spectrum (SRS) levels of a shock table under varying conditions. To achieve this, the study will investigate several critical aspects, including the effectiveness of different transient response analyses within FEM simulations, the influence of modelling techniques on the precision of SRS predictions, and the impact of various parameters on the resulting SRS, such as plate size, material properties, impact velocity, and boundary conditions.

1.2. Methodology

The development of a shock table using finite element analysis (FEA) to predict Shock Response Spectrum (SRS) levels requires a structured approach that integrates conceptual design generation, parametric studies and a design space exploration phase. The methodology employed in this study ensures that each stage contributes to the overall objective of evaluating the accuracy of FEA in predicting shock responses while identifying key factors influencing the system's performance in order to develop a functional shock testing facility.

The initial phase of the study involves the conceptual design generation, where multiple design alternatives are proposed based on insights from the literature review. This phase serves to establish a foundation for selecting a viable shock table configuration that aligns with performance requirements and practical constraints. The initial elimination process of these concepts is based on qualitative reasoning, taking into account key requirements established by the stakeholders and overall feasibility. Following this, the remaining concept designs are subjected to a more structured decision-making process, which is implemented using the Analytic Hierarchy Process (AHP), executed in MATLAB. The AHP method allows for a systematic evaluation of the remaining design candidates by comparing them against each other on key criteria such as cost, performance, and other relevant factors defined by the stakeholder's priorities. The outcome of this phase is the selection of a concept design that serves as the basis for further numerical investigations.

After selecting the conceptual design, the study moves to the simulation phase, where finite element models are created in MSC Nastran to evaluate the system's dynamic response. This phase focuses on assessing how different modelling approaches influence the accuracy of SRS predictions and computational efficiency. Models of varying levels of detail are constructed to investigate the trade-off between computational cost and result accuracy. Additionally, two distinct transient solution methods, direct transient and nonlinear implicit transient analysis, are employed to evaluate their respective capabilities in capturing shock behaviour. By systematically analysing these factors, this phase provides critical insights into the influence of model complexity, solver selection, mesh size, and time step on the fidelity of the results.

Following this, a study to examine the effect of key design parameters on the resulting SRS levels is conducted. This analysis considers variations in impact velocity, hammer and anvil characteristics, test specimen characteristics, and anvil material and measurement location. By exploring the impact of these parameters, the study assesses whether the FEA methods employed can reliably capture their influence on the shock response and whether the observed trends align with theoretical expectations. Understanding these relationships is essential for ensuring that the computational framework developed in this study can serve as a predictive tool for shock table performance.

The final stage of the methodology involves design space exploration, where numerical simulations are utilised to refine the shock table configuration in order to achieve an SRS profile that meets the target specifications provided by the launcher. This process involves systematically adjusting key model parameters to replicate the desired SRS within predefined tolerances. Successfully matching the simulated SRS to the target values provides valuable insights into the required test setup and system configuration. The configurations that achieve the expected SRS are then used to inform final design decisions, ensuring the shock table meets performance requirements while considering practical constraints.

Through this structured methodology, the study systematically investigates the accuracy of finite element models in predicting shock responses, evaluates the influence of critical modelling choices, and explores the effects of key design parameters. The findings from these analyses contribute to the refinement of the shock table design and provide a foundation for guiding future experimental implementations.

2

Concept Design

The concept generation phase is a crucial part of any project, where multiple concepts are explored to tackle the proposed project objectives effectively. During this phase, various concepts are considered and evaluated to determine their feasibility, applicability, and whether they comply with the requirements. This is an iterative process which aims to refine the concept designs through various modifications.

The designs are evaluated both individually and comparatively with each other, which will start the elimination process. The remaining options are then further developed with a higher level of detail and compared until only a few or just one possible design remains. As such, the primary goal of this phase is to establish a solid foundation for the design that will be implemented in the project through iterative evaluation and refinement. Therefore, it is important that, before starting this process, the requirements of the design of the shock testing facility are well defined, as they will greatly influence and guide the choices made in selecting a final concept design.

2.1. Requirements

The project requirements serve as guiding principles throughout the entire design and development process, ensuring that the final solution meets the intended objectives and aligns with stakeholder expectations. A clear and precise definition of these requirements is vital to the project's success.

The requirements for this project have been categorised into two groups: stakeholder requirements and system requirements [23]. This division was made in order to better understand and manage project constraints and objectives, as stakeholder requirements guide the development of user-centric solutions, while system requirements ensure that the technical aspects meet industry standards.

Stakeholder requirements represent the needs and expectations of those directly involved or impacted by the project [23]. These requirements focus on the functional aspects of the shock table, including its testing capabilities, payload capacity, budget constraints, and physical space requirements.

To better organise and communicate these requirements, they have been summarised in Table 2.1. This table provides a clear overview of each requirement, including a unique code for easy reference, a concise description of the requirement, and the rationale explaining its significance to the project.

On the other hand, system requirements focus on the technical specifications and performance criteria needed to ensure the effective operation of the shock table, supporting the stakeholder requirements from a technical standpoint [23]. These requirements address the structural integrity, repeatability of shock conditions, and data acquisition capabilities of the system. Fulfilling these requirements ensures the development of a shock table that is durable, reliable, and capable of producing consistent test results.

The system requirements defined for the development of the shock table are summarised in Table 2.2. This table provides a detailed overview of the technical requirements, along with the rationale for their

Table 2.1: Stakeholder Requirements and Rationale

Code	Requirement	Rationale
S1	Capable of testing heavier payloads, ideally up to 50 kg.	Ensures that the shock table can accommodate a wide range of testing applications, as payloads of this mass are commonly encountered in industry. This impacts the structural design, requiring robust construction to handle the additional load and associated forces during testing.
S2	Accommodates payloads measuring up to 350 mm x 350 mm.	Defines the dimensions of the test platform to ensure it fits the typical size range of test specimens. This requirement affects the overall layout and spatial constraints of the shock table, as well as the design of the support structure.
S3	Achieves the required excitation levels for the Falcon 9 launcher defined in [5].	Ensures the shock table can generate sufficient force to meet testing standards, enabling accurate simulation of real-world shock events for various payloads. This drives the selection and design of the actuation mechanism.
S4	Manufacturing and assembly costs fit within budget constraints of 2500€.	Maintains the project's financial feasibility, requiring trade-offs in material selection, actuation mechanism, and manufacturing complexity to balance cost with performance.
S5	Fits within the designated 2m x 2m housing and operational space.	Ensures the shock table can be installed and operated in the available space, avoiding the need for costly facility modifications. This imposes constraints on the table's size and layout.

inclusion in the design process. Meeting these requirements is essential for developing a shock table that is durable, reliable, and capable of producing consistent test results.

Table 2.2: System Requirements and Rationale

Code	Requirement	Rationale
T1	Durable and stable structure to withstand repetitive shock loading.	Ensures the shock table can endure both the setup and repeated test shocks, which involve a series of high-intensity impacts during calibration and testing phases. These shocks are characterised by extremely high accelerations (exceeding 1000g), requiring the table to maintain its structural integrity and functionality over multiple shock events without degradation.
T2	Repeatability of shock conditions.	Guarantees consistent and accurate reproduction of shock events, which is critical for achieving reliable test results and ensuring the validity of experiments and validations.
T3	Data acquisition system capable of recording accurate and high-resolution test data.	Allows for precise measurement of critical parameters during testing, ensuring accurate representation of the shock event. The system must also withstand the high accelerations and vibrations of the shock environment without losing data integrity.

2.2. Concept Generation

In order to generate the possible designs for the shock table, thorough consideration was given to the current state of the art in shock testing technology. This involved an in-depth analysis of existing methodologies, equipment, and best practices within the field, which were mentioned in the literature review section.

The concept design for the shock table development was structured around three main categories that play a role in determining the functionality and effectiveness of the shock table: the impactor, the resonant fixture, and the connection to the environment. These categories collectively define the

table's core functionality, as they determine how shock loads are applied, transmitted, and isolated during testing.

First, the impactor category which involves the various mechanisms used to deliver shock loads to the test specimen. The impactor must be capable of delivering precise and consistent shock inputs to the test specimen while ensuring safety and reliability. As such, the selection process for the impactor is driven by factors such as cost-effectiveness, ease of implementation, power delivery capabilities, repeatability of shock conditions, recharge time, and overall practicality. The options considered for the impactor are pendulum hammer [3], drop weights [12], pneumatic piston [11], explosives [10], laser [15] and nail gun [6].

Next, the resonant fixture category refers to the structure on which the test specimen is mounted during shock testing, which directly influences the transmission and amplification of shock waves to the test specimen. It must ensure structural integrity, compatibility with varying payload sizes and weights, and well-defined resonance characteristics. Therefore, when selecting the resonant fixture, considerations such as structural integrity, compatibility with the test specimen size and weight, and resonance characteristics are paramount, as it must be robust enough to withstand repetitive shock loading while providing a stable and controlled testing environment. The options considered for the resonant fixture for the shock table being developed are a bar [8], a beam or a plate [2].

Lastly, the connection to the environment category encompasses the means by which the shock table interacts with its surrounding environment. This is a vital part of the shock table as it is responsible to ensure its stability and isolation from external vibrations or disturbances, thus ensuring consistency in testing conditions. The options considered in this category include the resonant fixture hanging with cords, resting on foam pads, and secured with clamping mechanisms, and the selection process is influenced by factors such as space constraints, ease of setup, and the desired level of isolation from external influences.

By systematically considering all options within the three categories, a total of 54 potential designs were identified. These combinations are summarised in the design tree shown in Figure 2.1, which visually represents the approach taken during concept generation. This tree served as a foundation for the evaluation and refinement of the designs in subsequent phases.

With a multitude of possible designs, the next step involved systematically narrowing down the options to identify the most viable solutions. This was achieved through a rigorous evaluation process, eliminating designs that failed to meet critical requirements or posed significant practical challenges.

The initial phase of the elimination process consisted of a comprehensive evaluation of all the options for each category. These qualitative evaluation not only consisted of how well the solution met the requirements but also other critical factors that have previously been mentioned as relevant for each category.

Table 2.3: Impactor Options.

Option	Cost	Implementation	Power	Repeatability	Recharge Time	Practicality
Pendulum Hammer	Cheap	Easy	Good	Good	Fast	Practical
Drop Weight	Cheap	Easy	Good	Good	Fast	Practical
Pneumatic Hammer	Expensive	Medium	Good	Good/Okay	Medium	Practical
Explosives	Very Expensive	Very Complex	Very Good	Variable	Long	Not Practical
Laser	Expensive	Complex	Good	Good	Medium	Not Practical
Nail Gun	Cheap	Easy	Good	Medium	Medium	Medium Practical

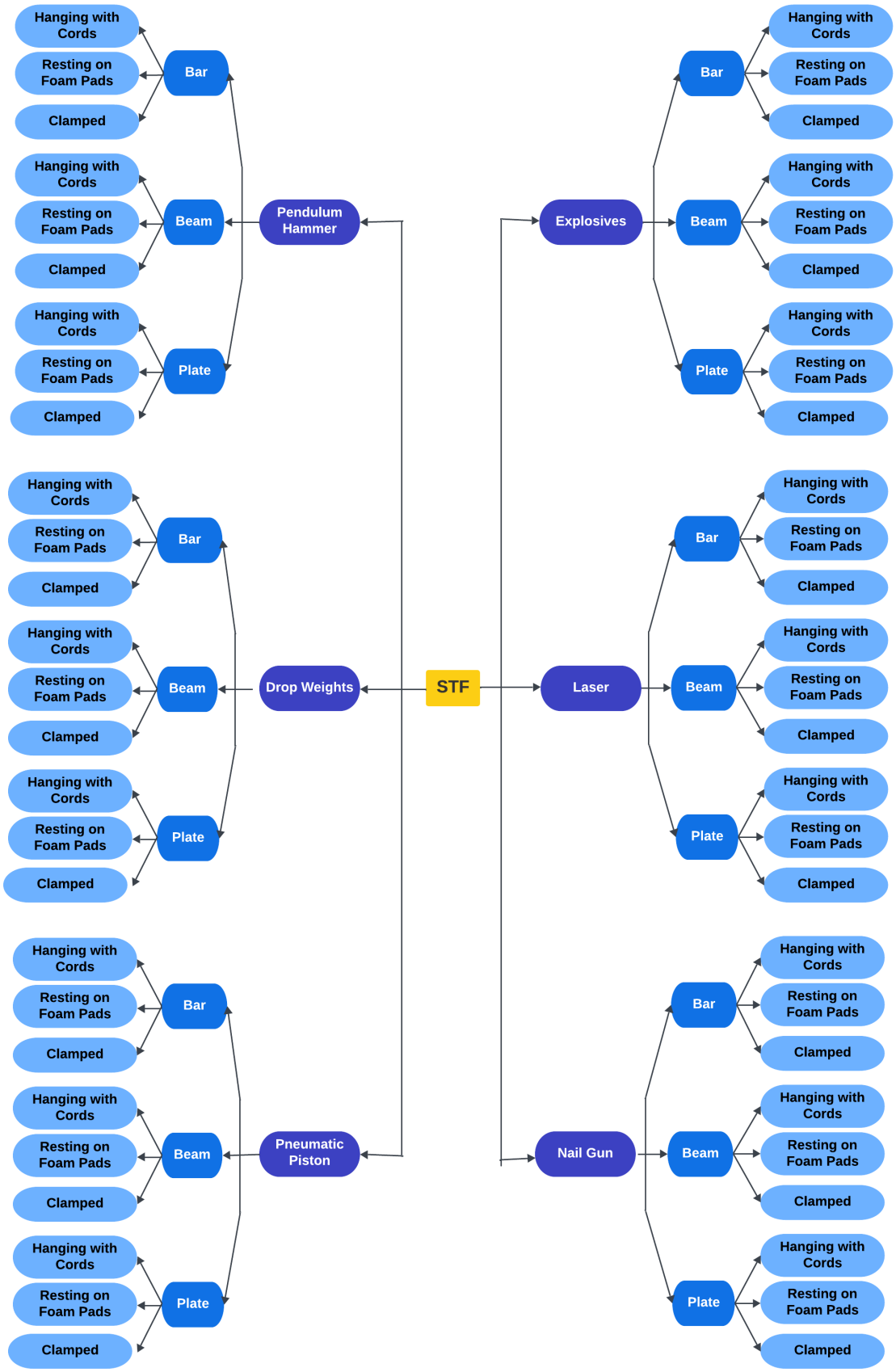

Figure 2.1: Concept Design Tree.

Starting with the evaluation of the impactor options shown in Table 2.3, each option was evaluated in regard to their cost, the ease of their implementation, their power capacity, ability to produce repeatable results, required downtime between tests, and overall practicality. This simple evaluation revealed that some options were not viable solutions and were therefore eliminated.

For example, the use of explosives was quickly dismissed due to its extremely high cost, complex implementation process, and impracticality in achieving consistent results [4]. This option fails to meet requirement S4 (budget constraints) due to its high cost and difficulty in ensuring repeatable performance and requirement T2 due to the complexity of repeating results.

Similarly, the laser option was excluded as a possible impactor, mainly due to its impracticality and complex implementation [15]. This approach requires highly specialised equipment, such as high-energy pulsed lasers and precise targeting systems, which demand complex setup procedures and strict safety measures [15]. Additionally, it does not satisfy requirement S4 (cost constraints), as it would involve significant investment in equipment and operational infrastructure.

The nail gun was also discarded, as it is known for spreading a lot of particles, potentially posing logistical challenges [3]. This approach does not align with S5 (fit within the operational space and conditions), as the spread of particles would introduce significant operational difficulties and contamination risks. However, it was noted that the nail gun could still be considered for future updates to the shock test facility.

A similar evaluation was conducted for the selection of the resonant fixture. The plate was determined to be the most viable solution, as bars and beams lack the necessary surface area and mechanical stability to support the required payloads. The shock levels specified for the Falcon 9 launcher include a 1000 Hz knee frequency, meaning that the bar must have a first longitudinal natural frequency of 1000 Hz [4]. Using Equation 2.1 and Equation 2.2, a bar would need to have a length of approximately 2.55 m to achieve this requirement.

A bar of this length would far exceed the available space constraints (requirement S5). Additionally, the shock table must accommodate specimens measuring up to $350\,\text{mm} \times 350\,\text{mm}$. An aluminium bar with a length over 2.5 m and a cross-section of $350\,\text{mm} \times 350\,\text{mm}$ would not only be difficult to procure, but it would also exceed the budget constraints, breaking requirement S4. Therefore, a plate was selected as the most appropriate resonant fixture for further development.

$$c = \sqrt{\frac{E}{\rho}} \tag{2.1}$$

$$l = \frac{c}{2f} \tag{2.2}$$

where:

- c = longitudinal wave speed (m/s)
- E = Young's modulus of aluminium, $70\,\text{GPa}$
- ρ = density of aluminium, $2700\,\text{kg/m}^3$
- l = required bar length (m)
- f = desired first longitudinal mode frequency, $1000\,\text{Hz}$

Lastly, for the connection to the environment, only configurations involving hanging with cords and resting on foam pads were considered as different options for the design, as the inclusion of clamps could always be added to the chosen design without requiring a separate evaluation process [3].

After the initial elimination process, four designs remained and were considered the most viable options, which required further development:

- Design 1 - Horizontal Plate with Pendulum Hammer
- Design 2 - Horizontal Plate with Drop Weights

- Design 3 - Vertical Plate with Pendulum Hammer
- Design 1 - Horizontal Plate with Pneumatic Piston

2.2.1. Design 1 – Horizontal Plate with Pendulum hammer

The first possible design features a plate as a resonant fixture, paired with a pendulum hammer as an impactor. The plate is supported by resting horizontally on foam pads. Figure 2.2 shows a simple representation of the main features of this concept design.

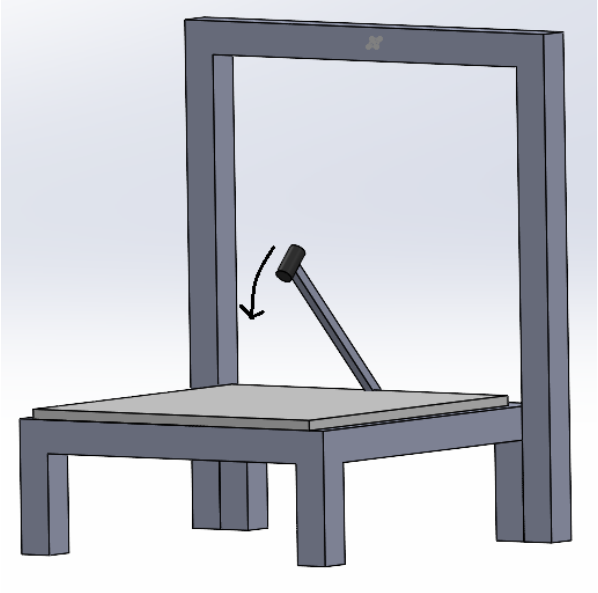

Figure 2.2: Concept Design 1 – Pendulum Hammer with Horizontal Plate.

This design offers a cost-effective and straightforward solution for shock testing, as it is easy to implement and operate while providing repeatable results with low reload times.

However, size limitations due to the available space may restrict the impact power of the STF. Achieving higher impact velocities requires increasing the height from which the pendulum is dropped, as the relationship between height and impact velocity is quadratic. This means that even small increases in velocity lead to disproportionately larger apparatus sizes. For example, with the available horizontal space limited to 2m × 2m (requirement S5) and a 1m × 1m plate positioned centrally, the maximum length for the pendulum hammer would be constrained to 1.5m. With this setup, the maximum achievable impact velocity would be approximately 5.42 m/s, assuming the pendulum hammer is released from the maximum height of 1.5m. Consequently, the available operational space directly limits the maximum height for the pendulum hammer, which in turn limits the achievable impact velocity and, ultimately, the STF's overall performance.

2.2.2. Design 2 – Horizontal Plate with drop weights

The second concept design considered consists of a plate as a resonant fixture, paired with drop weights as the impactor. Similar to the first design, the plate is supported horizontally on foam pads. A visual representation of this design is provided in Figure 2.3.

This design shares similar advantages with the first one, also offering a cheap and simple solution to the shock table development. Nonetheless, one notable disadvantage is the significant increase in apparatus size vertically with impact velocity. Due to the quadratic relationship between the drop height and the impact velocity, achieving higher velocities requires much greater heights for the drop mechanism. For example, to achieve an impact velocity of 5 m/s, the drop height must be approximately 1.3 m, as calculated in Equation 2.4. If we consider that the plate is positioned around 0.5 m above the ground, the overall structure would need to be nearly 2 m tall.

Although the requirement for available space defines constraints only in the horizontal direction, vertical

space is not unlimited. Extremely tall setups, such as those exceeding a few meters, can introduce practical challenges. These include limitations on the maximum impact velocity, structural stability concerns, and the need for additional very tall infrastructure to raise and reset the weights after each drop.

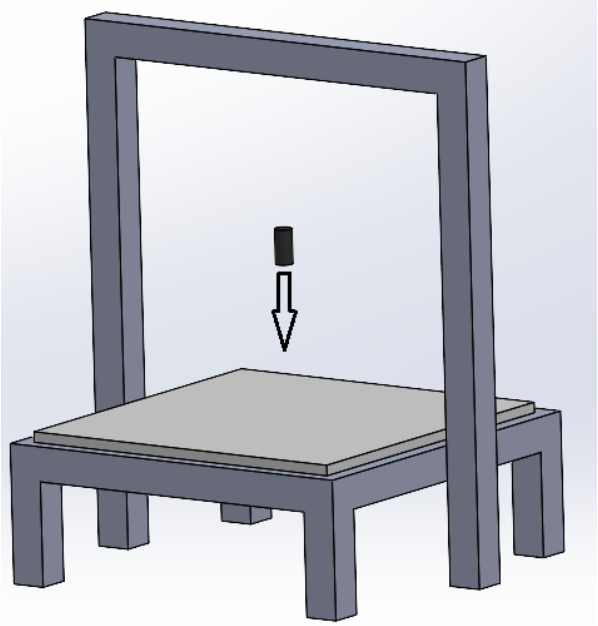

Figure 2.3: Concept Design 2 – Horizontal Plate with drop weights.

2.2.3. Design 3 – Vertical Plate with Pendulum Hammer

The third possible design also features a plate as a resonant fixture, paired with a pendulum hammer as an impactor. However, unlike the previous designs the plate in this concept suspended vertically by cords. Figure 2.4 presents a simple representation of this design.

The advantages of this design are similar to the previous ones, as it also provides a cost-effective and easy-to-operate solution for shock testing [1]. Moreover, the vertical suspension offers a key advantage: it allows the pendulum hammer to be dropped from an angle approaching 180º relative to the surface of the plate. In contrast, a horizontal plate configuration restricts the pendulum drop angle to a maximum of 90º. This means that for the same pendulum arm length, the vertical configuration can effectively double the drop height, allowing for higher impact velocities and greater impact power without requiring additional horizontal space. This efficient use of space makes the vertical setup particularly advantageous when space is limited. For example, in the case of the horizontal plate design (Design 1), the available horizontal space restricts the pendulum hammer length to a maximum of 1.5m, resulting in a maximum achievable impact velocity of approximately 5.42 m/s. However, with the vertical configuration, the drop height can be increased to 3m for the same arm length, resulting in a higher achievable impact velocity of approximately 7.67 m/s, leading to greater overall performance.

Lastly, the vertical suspension allows for a different test setup, making it possible to conduct tests on specimens in an upright configuration. This can be advantageous when simulating certain shock scenarios where a specific upright orientation of the specimen plays a critical role.

Nevertheless, the ability to mount large and heavy equipment onto the plate to be tested and the stability of the structure itself may be compromised due to the hanging configuration. While it allows for a unique test setup, the suspended plate can sway or vibrate excessively, potentially leading to inconsistent results or difficulty in securing heavier payloads, as established in requirement S1.

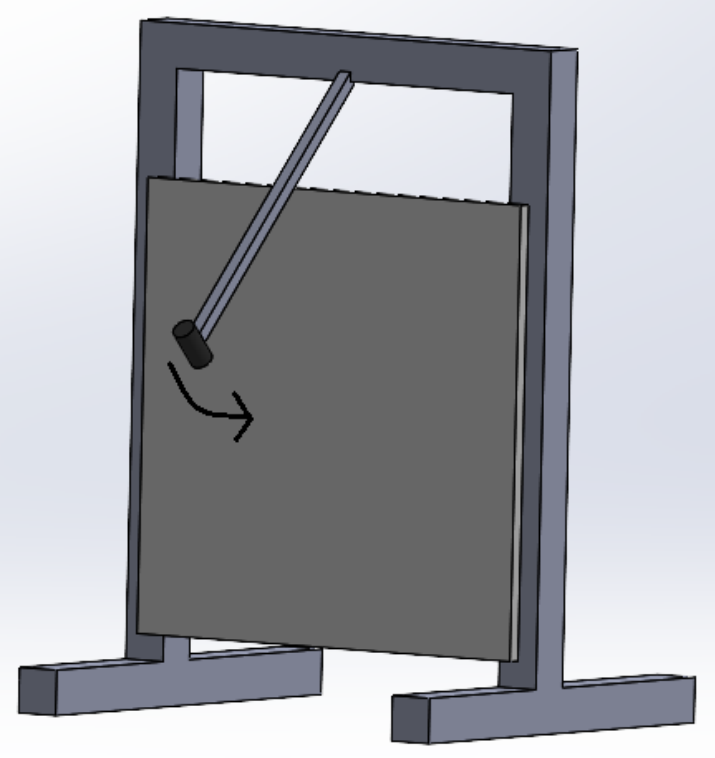

Figure 2.4: Concept Design 3 - Vertical Plate with Pendulum Hammer.

2.2.4. Design 4 - Horizontal Plate with Pneumatic Piston

The fourth and last possible design comprises a plate as a resonant fixture, paired with a pneumatic piston as the impactor. Similar to some previous designs, the plate is supported horizontally on foam pads. Figure 2.5 illustrates the main features of this concept design.

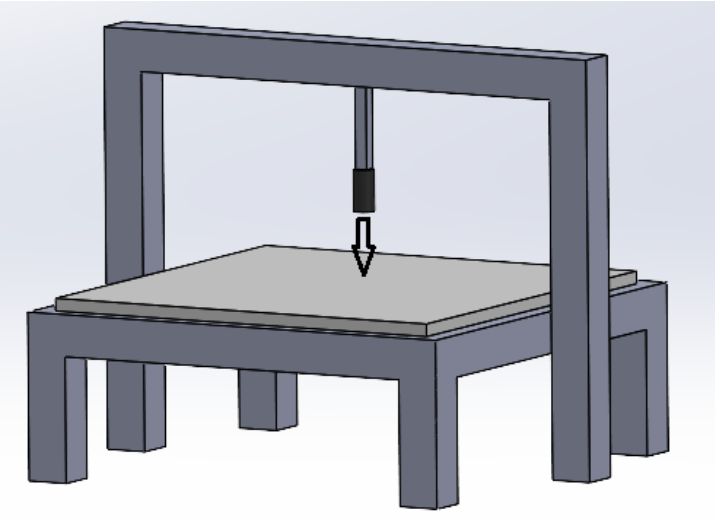

Figure 2.5: Concept Design 4 - Horizontal Plate with Pneumatic Piston.

The main advantages of this design are its compact size and its ability to deliver relatively high impact energy compared to the other concepts considered [11]. However, it also presents certain disadvantages. In particular, the use of a pneumatic piston requires a compressor, which typically involves a recharging period between activations. While high-performance compressors can minimise this delay, they are often too expensive. More affordable options tend to have longer recharge times, which could

reduce the efficiency of the shock table by reducing the number of shocks that can be delivered in a given period.

In addition, the overall cost of the system may be significantly higher than other concepts. Beyond the compressor itself, additional components such as the piston, control valves, and necessary fittings add to both complexity and expense. As a result, the design may not meet the cost-related constraint defined in requirement S4.

2.3. Detailed Concept Design

The four proposed concept designs share certain key elements while differing in their impactor mechanisms and methods of connecting the resonant fixture to the environment. These shared considerations ensure that all designs meet the project's functional and durability requirements.

By impacting directly the plate, this will damage it. Since the resonant plate will be one of the more costly components of the STF, it is important to ensure that the plate can sustain a large amount of shocks. As such, all the concept designs considered will encompass an anvil plate, which will be impacted instead of the resonant plate. This sacrificial plate is rather small, making it easier and cheaper to replace, and since less material is used, it is also more sustainable.

Clamps are an optional feature that can be added to all designs to secure the plate during testing. While the specific method of incorporating clamps may vary depending on the design, they provide additional stability and flexibility, allowing for more controlled and varied testing conditions.

While the supporting structures of each design are different, all the options considered share a common requirement: stability. To ensure accurate test results, all structures will be securely anchored to the floor to prevent displacement or movement during impact.

Additionally, all supporting structures will be constructed from aluminium profiles. This choice balances strength and weight while also ensuring ease of assembly and adaptability to design modifications.

2.4. Analytic Hierarchy Process (AHP)

From the different concepts that were created and presented, a final design will be chosen using the Analytic Hierarchy Process (AHP). This approach to decision-making allows a better understanding of the problem as it is decomposed into an hierarchy of more tangible and easily understandable sub-problems [24].

AHP has been widely applied in various fields, including economics, social sciences, and engineering, where complex decisions must balance multiple criteria [24]. In engineering, AHP aids in linking technical specifications with stakeholder values, offering a clear framework for informed decision-making.

The first step to apply it is to define the criteria under which the four possible designs considered will be evaluated. The criteria chosen are stability, power by size, practicality/complexity, cost, ease of mounting specimen, and time between tests. These criteria will be further explained below, once the designs are evaluated.

But first it is necessary to establish the importance of the criteria, as some weigh more in the decision-making process than others. The weights of these criteria were determined based on the company's priorities and requirements, ensuring that the final design aligns with the business's strategic goals and operational constraints. Table 2.4 presents the relative importance of each evaluation criterion used for selecting the shock table design. Among these, cost is considered the most important factor in the selection of the shock table due to the tight budget that must be adhered to. Ease of mounting the specimen, while still important, is considered the least critical factor.

Once the weight of the criteria has been evaluated, the next step is to evaluate how each design performs in each criteria in relation to each other.

2.4.1. Stability

Starting with stability, this criterion is the ability of the shock table to remain stable upon impact, ensuring no significant movement that could interfere with test results. This is related to system requirement

Table 2.4: Criteria Evaluation.

Criterion / Criterion	Stability	Power by Size	Practicality / Complexity	Cost	Ease of Mounting Specimen	Time between Tests
Stability	1	3	4	1/4	4	4
Power by Size	1/2	1	2	1/5	4	3
Practicality / Complexity	1/4	1/2	1	1/5	3	3
Cost	4	5	5	1	7	7
Ease of Mounting Specimen	1/4	1/4	1/3	1/7	1	1/3
Time between Tests	1/4	1/3	1/3	1/7	3	1

T1, which emphasises the need for a durable and stable structure that can withstand repeated shock loading.

Table 2.5 presents a comparative analysis of the stability of the different design concepts. The values in the table represent the relative stability of each design in comparison to the others, with higher values indicating better stability.

Table 2.5: Stability

Design / Design	Design 1	Design 2	Design 3	Design 4
Design 1	1	1	4	1/3
Design 2	1	1	4	1/3
Design 3	1/4	1/4	1	1/6
Design 4	3	3	6	1

Design 4 was considered the most stable, largely due to its impactor which requires a smaller supporting structure. Its compact design reduces the likelihood of sway or unwanted movement, contributing to its overall stability. In contrast, Designs 1 and 2 require taller supporting structures, which increase the potential for instability [4]. While these designs remain structurally sound, their taller supports can amplify the effects of dynamic forces during shock loading, making it more challenging to achieve the same level of stability. However, it is important to note that this does not imply these designs are unstable their stability is just comparatively lower than that of Design 4. Design 3 is considered the least stable due to its vertically suspended plate, which is more prone to movement during shock loading [1]. The suspension setup makes it susceptible to sway or oscillation, posing challenges for maintaining consistent stability, especially during high-impact tests.

2.4.2. Power by size

The next criterion analysed is power by size, which refers to the size of the shock table required to achieve a desired impact velocity. This criterion is closely tied to both Stakeholder Requirement S5, which specifies that the shock table must fit within the designated housing and operational space, and Stakeholder Requirement S3, which ensures the shock table can achieve the required excitation levels. Larger designs may offer higher impact velocities and better excitation levels, but they also require more space, potentially impacting the design's ability to meet spatial constraints.

Table 2.6 shows how each design was evaluated in relation to one another based on this criterion. The values in the table represent the relative power-to-size efficiency of each design, with higher values indicating a more efficient use of the supporting structure's size to achieve the desired impact velocity.

Once again, design 4 is considered the best option. The pneumatic piston system in this design does not require a large supporting structure, allowing it to achieve high impact velocities without increasing

Table 2.6: Power by Size

Design / Design	Design 1	Design 2	Design 3	Design 4
Design 1	1	1/2	1/2	1/5
Design 2	2	1	1/2	1/4
Design 3	2	2	1	1/2
Design 4	5	4	2	1

the overall size. This advantage gives Design 4 the highest ranking in this category. The remaining designs rely on gravity to generate the required impact force. Consequently, to achieve higher impact velocities, these designs require the impactor to be dropped from greater heights, which increases the size of the shock table significantly. Using the mechanical energy equation shown below, this relation between impact velocity and size of the structure was studied.

$$E = mgh + \frac{1}{2}mv^2 \tag{2.3}$$

$$h = \frac{v^2}{2g} \tag{2.4}$$

Figure 2.6 shows that the height from which the impactors have to be dropped increases quadratically in regard to the impact velocity. This means that the designs powered by gravity require bigger supporting structures to function. Consequently, these designs are rated lower for power by size. In particular, Design 1 and Design 2 are ranked similarly, with Design 1 receiving a slight advantage due to its simpler gravity-powered mechanism. Design 3, while slightly better than the other two in terms of size-to-power ratio, is still constrained by its reliance on gravity for power.

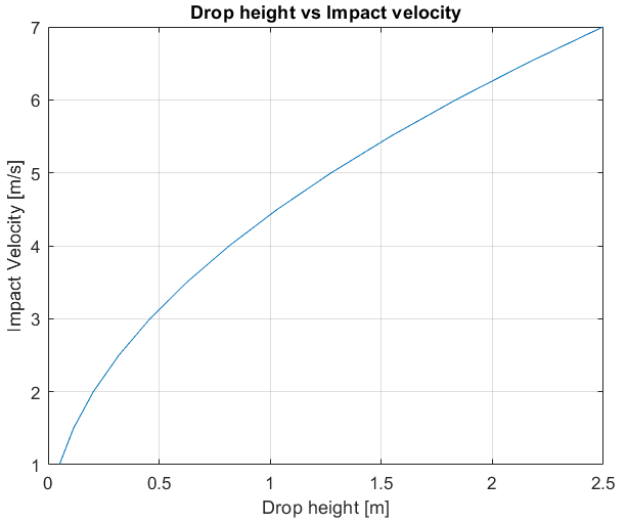

Figure 2.6: Hammer drop height vs Impact velocity.

2.4.3. Practicality / Complexity

The next criterion evaluates the ease of operating the shock table and how complex implementing its design is. Table 2.7 shows how each design was evaluated in relation to one another based on this criterion. Once again, the values in the table represent the relative practicality and complexity of each design in comparison to the others, with higher values indicating more practicality and less complexity.

It is clear the fourth design is both the most complex to implement as well as the hardest to operate. To work with the pneumatic piston, a system has to be integrated, including compressors and valves, making it both harder to implement and operate [11]. On the other hand, the other designs rely solely

Table 2.7: Practicality / Complexity

Design / Design	Design 1	Design 2	Design 3	Design 4
Design 1	1	3	4	6
Design 2	1/2	1	2	4
Design 3	1/4	1/2	1	3
Design 4	1/6	1/4	1/3	1

on gravity, meaning it is only needed to reposition the impactor in order to operate the shock table [12]. Design 1 was considered slightly more practical than the other two due to the ease of setting the impactor in its original position. For design 2, if the weights are dropped from too high up, it will be harder for the user to set it up as other mechanisms may be needed. For design 3 this also applies for set ups were the pendulum hammer is dropped from great heights.

2.4.4. Cost

As previously mentioned, this is the most important parameter in the decision-making process due to the impossibility of going over budget. The Cost criterion evaluates the financial feasibility of each design, which is directly tied to stakeholder requirement S4. The performance of each design is shown in Table 2.8, with higher values representing more cost-effective solutions.

Table 2.8: Cost

Design / Design	Design 1	Design 2	Design 3	Design 4
Design 1	1	1/2	1/2	6
Design 2	2	1	1	7
Design 3	2	1	1	7
Design 4	1/6	1/7	1/7	1

Design 4 is the most expensive, primarily due to the inclusion of a pneumatic piston. This system requires various components such as compressors and valves, which significantly increase the overall cost. Despite having a smaller supporting structure, the additional equipment required for the pneumatic system makes Design 4 the most costly option.

2.4.5. Ease of Mounting Specimen

Ease of Mounting Specimen is an important criterion, as the shock table must accommodate test specimens that can vary in size and weight, as specified in requirements S1 and S2. The mounting process should be as straightforward as possible, especially when dealing with large and heavy test specimens. Table 2.9 shows how each design was evaluated in relation to one another based on this criterion.

Table 2.9: Ease of Mounting Specimen

Design / Design	Design 1	Design 2	Design 3	Design 4
Design 1	1	1	5	1
Design 2	1	1	5	1
Design 3	1/5	1/5	1	1/5
Design 4	1	1	5	1

In this regard, Design 3 presents the greatest challenge, as the vertical mounting configuration makes it difficult to handle large specimens [1]. This design's suspended structure could complicate the process, which is why it scores the lowest in this criterion. On the other hand, Designs 1, 2, and 4 are all quite similar in terms of mounting ease, as they feature a simple and accessible horizontal setup.

2.4.6. Time between Tests

Shock tests take time to set up. Due to the various factors at play in a test, the parameters of the shock table have to be fine-tuned to produce the desired SRS curve. To achieve this, generally, multiple tests have to be made until the correct setup is found in order to prevent under and over-testing of the test

specimen. Consequently, it is important to be able to make consequent tests without a lot of downtime.

As such, Time between Tests is a key factor in evaluating the efficiency of the shock table and Table 2.10 shows how each design fared against each other.

Table 2.10: Time between Tests

Design / Design	Design 1	Design 2	Design 3	Design 4
Design 1	1	2	4	8
Design 2	1/2	1	1/2	7
Design 3	1/4	2	1	5
Design 4	1/8	1/7	1/5	1

Due to the impact method for designs 1,2 and 3, it is relatively quick to conduct consequent tests, as the only thing that needs to be done is put the impactor in the desired position. For the fourth design, the process is more complicated, since the use of a pneumatic piston requires a compressor to operate. Since the compressor needs to be recharged between tests, it adds significant downtime to the testing process. While state-of-the-art compressors could speed up this process, such equipment is outside the budget constraints of this project. Consequently, Design 4 is slower in comparison to the other designs.

2.4.7. Final Design Scores

After applying the Analytic Hierarchy Process (AHP), each design was given a final score, reflecting its overall performance based on the predefined criteria. The global priorities presented in the table were obtained by first calculating the individual scores for each design based on their performance in each of the selected criteria. These individual scores were then multiplied by the weights assigned to each criterion, reflecting their importance in the overall decision. The weighted scores were summed up to obtain the global priority for each design [24].

These scores are presented in Table 2.11, with Design 2 emerging as the highest-scoring option, followed closely by Design 1. Design 3 and Design 4 scored slightly lower, with Design 4 being the least favourable.

Table 2.11: Global Priorities for Each Design

Design	Global Priority
Design 1	0.2468
Design 2	0.2845
Design 3	0.2459
Design 4	0.2229

Design 2 was identified as the preferred solution, primarily due to its balanced performance across key criteria. It provides a good compromise between stability, power by size, and ease of mounting specimens. Additionally, the simplicity of the design ensures that it remains practical and cost-efficient, especially in terms of operational complexity and time between tests.

Although Design 2 has the highest score, the decision is not entirely final because the results from Finite Element Method (FEM) simulations could still influence the final choice. Therefore, while it is still considered the preferred option, the remaining designs are not completely excluded, especially due to the marginal differences in the score.

3

Parametric Studies

Simulations can play a crucial role in the design and optimisation of shock testing facilities. As all proposed designs feature a plate as the resonant fixture, simulations offer a systematic approach to evaluate design parameters and refine configurations to meet performance requirements. By providing insights into material selection, impact velocity determination, and overall design optimisation, simulations can serve as a valuable tool in the decision-making process.

3.1. Initial Considerations

Before proceeding with simulations, it is crucial to establish the initial configurations for key components of the shock table, including the plate, impactor, and anvil. Defining these baseline parameters ensures a consistent simulation framework and enables a systematic study of how individual variables affect the resulting Shock Response Spectrum (SRS).

Although many factors influence the SRS produced by the shock table, not all are easily or practically adjustable. Therefore, certain parameters are held constant throughout this study, as modifying them would involve substantial changes to the physical shock testing facility. For example, the resonant plate is kept constant because it is the most costly component of the selected shock table design. Varying this part would not only result in significant expense but would also involve considerable effort in physically replacing a large and heavy structure. Similarly, the mounting location of the test specimen is fixed, as the table is designed to accommodate large and heavy payloads, making repositioning during calibration labor-intensive and inefficient.

Instead, this study focuses on parameters that are relatively easy to modify in practice and have a notable influence on the SRS shape and amplitude. These include:

- Impact velocity
- Impactor mass and material
- Anvil thickness and material
- Test specimen mass

By varying these parameters, the simulations aim to provide valuable insights into how the design can be fine-tuned to meet performance requirements and produce desired shock environments. The next step is then to determine the parameters that will remain constant and define the baseline values for those that will be varied during simulation.

3.1.1. Plate Sizing

As previously mentioned, the plate is the most expensive component of the STF, and as such, it is impractical to have variations of the resonant fixture. Therefore, the plate will have a constant material, shape and dimension.

The initial sizing of the plate is crucial, as it directly impacts the SRS shape. Two common dimensions found in literature, 1m x 1m x 30mm and 1.22m x 1.88m x 13mm, are used as reference points [12][11].

To verify suitability, modal analysis was performed on both plate sizes to check for the presence of natural frequencies near the desired knee frequency of approximately 1000 Hz. Since the plate is supported on foam in almost all concepts, it was modelled using simply supported boundary conditions, meaning the plate was along the edges. Aluminium 7075 was the material chosen for both these plate and its mechanical properties can be seen in Table 3.1.

Table 3.1: Mechanical properties of Aluminium 7075-T6.

Property	**Value**
Young's Modulus (GPa)	71.7
Density (kg/m^3)	2650
Poisson's Ratio	0.33

The results obtained show that both plate sizes have significant modes around 1000 Hz, as presented in Table 3.2 and Table 3.3.

Table 3.2: Frequencies around 1000 Hz for a 1 m x 1 m Plate.

Mode	Frequency
7	947
8	947
9	1243
10	1243

Table 3.3: Frequencies around 1000 Hz for 1,22 m x 1,88 m Plate.

Mode	Frequency
206	996
207	997
208	1001
209	1002
210	1004

Since both plates have modes around the desired frequency, the plate with dimensions of 1m x 1m x 30mm was chosen as the plate size. This choice is supported by its successful use in similar applications [3], and its smaller, more standard dimensions help reduce material waste and overall manufacturing costs, making it the most practical and cost-effective option.

3.1.2. Impactor Sizing

In contrast to the resonant plate, the impactor is a component that can be modified relatively easily and at low cost. Adjusting the impactor's characteristics does not involve labour-intensive changes, and multiple hammers with different masses and materials can be fabricated and interchanged without significant disruption to the setup. This flexibility makes the impactor a practical and valuable parameter for tuning the shock table's SRS response.

The characteristics of the impactor, such as its mass, material, and shape, have a significant effect on the Shock Response Spectrum (SRS) [11]. For the purposes of this study, the material and mass will be the two parameters considered, while the shape is kept constant.

Titanium and steel were selected as candidate materials for the impactor. These materials are commonly used in shock testing literature due to their high stiffness, durability, and resistance to deformation under high-impact loads, making them suitable for reliable and repeatable impacts. The relevant material properties used in the simulations are listed in Table 3.4.

Table 3.4: Mechanical properties of candidate impactor materials.

Material	Young's Modulus (GPa)	Density (kg/m^3)	Poisson's Ratio
Titanium (Grade 5)	116	4500	0.342
Stainless Steel	190	7850	0.29

As a baseline, a titanium cylindrical hammer was selected with a diameter of 40 mm and a height of 100 mm. This configuration offers a good starting point due to its relatively low weight and durability, allowing for further mass adjustments.

To explore how impactor mass influences the SRS, modular weights will be used to increase the hammer's mass. Additional weights of 500 g and 1 kg can be attached to the baseline hammer, enabling systematic studies of mass variation effects without requiring a redesign or remanufacture of the impactor body.

3.1.3. Anvil Plate Sizing

Directly impacting the resonant plate would cause it to degrade over time, resulting in frequent and costly replacements. To address this issue, an anvil plate is used to absorb the direct impact from the hammer and protect the underlying resonant fixture.

Similar to the impactor, the anvil plate is a component that can be modified relatively easily in terms of material. In contrast, changing the shape or size of the anvil would require reworking the physical attachment and interface with the resonant plate, which is undesirable during iterative calibration. Therefore, the geometry of the anvil plate is kept constant throughout this study, while its material is varied to assess the effect on the resulting Shock Response Spectrum (SRS).

The materials selected for the anvil plate are aluminium and steel. These materials are commonly used in shock testing applications due to their mechanical strength, impact resistance, and availability. They also provide different stiffness and mass properties, allowing a useful comparison of how the anvil's material affects the impact characteristics. The relevant properties for simulation purposes are provided in Table 3.5.

Table 3.5: Mechanical properties of candidate anvil materials.

Material	Young's Modulus (GPa)	Density (kg/m^3)	Poisson's Ratio
Aluminium (7075-T6)	71.7	2650	0.33
Stainless Steel	190	7850	0.29

The initial design for the anvil plate consists of a 100 mm $\times$ 100 mm $\times$ 10 mm block, with four M6 holes included for attachment to the resonant plate.

3.2. Impact Analysis

This section explores how different FEA modelling approaches and levels of simulation complexity influence the accuracy and practicality of shock response predictions. The objective is to understand the trade-offs between model fidelity, computational cost, and the usefulness of simulation results during the development and calibration phases of the shock test facility.

The key focus of this study is transient dynamic analysis, which is essential for capturing the time-dependent behaviour of the system under impact loading. One of the most accurate and used methods for simulating shock events is the use of advanced non-linear explicit solvers. These are particularly well-suited for short-duration, high-intensity events like shocks, as they do not require solving a system of equations at each time step [2]. While explicit solvers typically require very small time steps for stability, this limitation is mitigated in shock analysis due to the brief duration of the events. As a result, explicit methods can often deliver faster performance than implicit methods for this type of simulation [2].

However, explicit solvers are not always readily available and are often associated with high licensing costs. Since MSC Nastran, the solver used in this project, does not support explicit dynamics, a non-linear implicit transient solution is adopted as the primary method. Although this approach is computationally more expensive, it allows for the inclusion of geometric and material non-linearities, leading to more realistic modelling of shock phenomena [2].

In parallel, a linear Direct Transient solution is also explored. This method assumes linear behaviour throughout the simulation, which simplifies the analysis but limits its ability to fully capture the physics of a shock event. Nevertheless, it is significantly more computationally efficient [25]. Comparing the two approaches will help assess the limitations of the linear method and identify conditions under which it may still yield acceptable results. This comparison will also provide insight into potential inaccuracies that might arise from relying solely on linear methods for shock analysis.

Additionally, the structure of the simulation models and the components included can influence the accuracy of the results. To explore this, simulations will be conducted with progressively increasing levels of model detail, starting with simplified configurations and gradually introducing additional components such as the anvil and test mass. This stepwise approach enables a clearer evaluation of how complexity affects both simulation fidelity and computational performance. Figure 3.1 outlines the planned simulation workflow and its corresponding levels of detail.

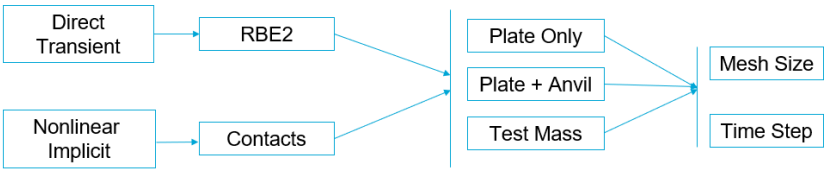

Figure 3.1: Level of detail in the simulations being performed.

The first set of simulations will use the Direct Transient method, with impact simulated via Rigid Body Elements (RBE2). These models will range from a basic configuration, containing only the resonant plate, to more complex configurations that include the anvil plate and test specimen. Each model will undergo mesh size and time step convergence studies to evaluate how these parameters influence simulation accuracy.

Subsequently, to increase the realism of the analysis, the non-linear implicit method will be applied. In this case, RBE2 elements will be replaced with contact definitions to simulate the impact more accurately. As before, each model in this series will be tested under varying levels of detail and subjected to convergence studies to ensure consistency and reliability in the results.

3.2.1. Direct Transient Analysis

The first set of simulations is performed using Direct Transient Analysis (SOL 103 and SOL 112 in Nastran), which solves the full coupled equations of motion over time without simplifying assumptions about the structure's response [25]. This method allows for the application of time-varying loads or the evolution of initial conditions, meaning it suits the impact event. By capturing the structure's time-history response, this approach provides detailed insights into the structures behaviour such as displacements, stresses, and accelerations at each time step [25], [26]. The acceleration time-history response is the interest in this analysis, since, as previously explained, this will then be used to get the SRS.

Since linear contact cannot be used in this analysis type, the impact is instead simulated using RBE2 elements. An RBE2 element is a rigid body constraint that enforces equal displacement at all its dependent nodes, making it a practical way to model an impactor while maintaining computational efficiency. In this setup, a mass element represents the hammer and is assigned a velocity as an initial condition, allowing the simulation to capture its effect on the structure as it evolves over time.

The models used with this analysis solution type will vary in detail, ranging from a basic model that includes only the resonant plate to more detailed models that include the anvil plate and test mass. Each of these models will undergo mesh size and time step convergence studies to evaluate the impact of these parameters on simulation accuracy.

To establish a baseline, the simplest possible configuration is first examined. Here, the resonant plate is modelled with 2D plate elements, and the impact is simulated with a mass element connected to the plate via an RBE2 element, with an initial impact velocity of 0.1 m/s, as shown in Figure 3.2.

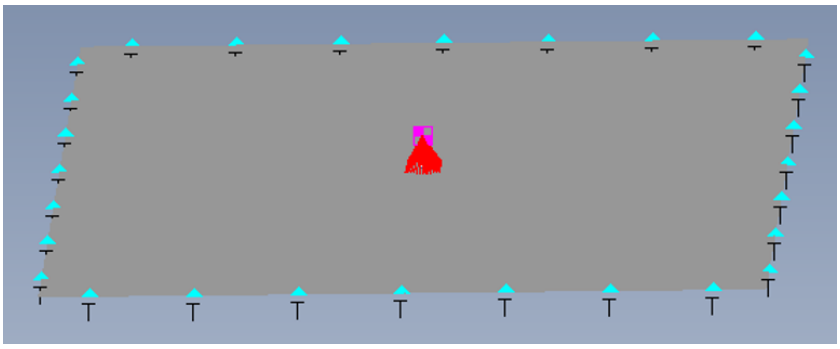

Figure 3.2: Model with RBE2 element connected to resonant plate only.

A convergence study was performed on two points of the resonant plate to establish a baseline for the number of elements required for accurate analysis. The plate was meshed using varying densities to assess the impact on simulation results. The mesh densities used in the study were:

- 50 elements by 50 elements, resulting in 20 mm element size
- 80 elements by 80 elements, resulting in 12.5 mm element size
- 100 elements by 100 elements, resulting in 10 mm element size
- 150 elements by 150 elements, resulting in 6.67 mm element size
- 250 elements by 250 elements, resulting in 4 mm element size

By systematically increasing the mesh density, the study aimed to identify the point at which further refinement no longer significantly improves the accuracy of the results. This approach ensures that the model is both computationally efficient and sufficiently accurate for the purposes of the shock analysis.

Additionally, two time steps were also considered, as it affects the accuracy of the simulations as well. The time steps used were 0.1 ms and 0.01 ms.

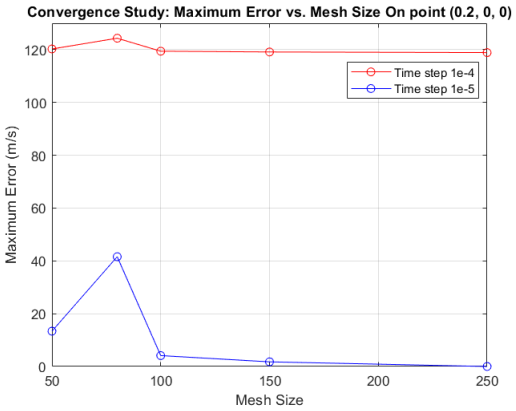

Figure 3.3: Convergence Study for Model with Plate Only for Point (0.2, 0, 0). Mesh Size is expressed in n x n elements.

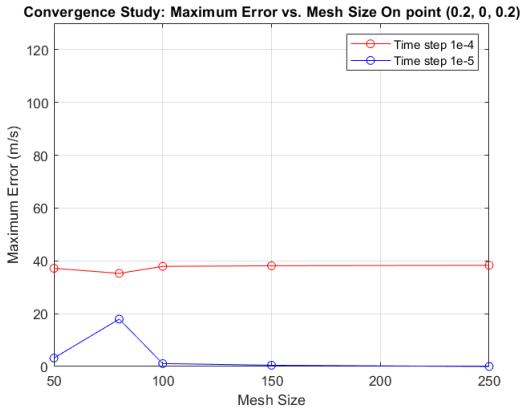

Figure 3.4: Convergence Study for Model with Plate Only for Point (0.2, 0, 0). Mesh Size is expressed in n x n elements.

Figure 3.3 shows the convergence study for the node situated at 0.2m of the centre of the plate in the horizontal direction. The graph clearly shows that the increase from 80 to 100 elements, actually increases the error found in the results. This is due to the previous mesh sizes being to big to capture

the behaviour of some of the higher frequencies. Additionally, the decrease in the time step also showed higher errors. The explanation for this behaviour is the same: when time steps are too big, they do not capture the behaviour of higher frequencies.

Figure 3.4 shows an identical behaviour to what was previously analysed. However, this point is further away from the impact point, at 0.2m distance from the centre of the plate in both axis, which explains why the errors are smaller. As the shock wave travels along the plate, the higher frequencies are dampened, leading to smaller errors, as they are the main source of them.

The same convergence study was then repeated to understand the effect of the time step and the mesh size in the frequency domain. As just seen, in the time domain, both the time step and mesh size significantly affected the acceleration response. However, this effect was less pronounced in the frequency domain using the Shock Response Spectrum (SRS) method. For brevity purposes, for the frequency domain, only the results obtained with the first point selected will be shown. Figure 3.5 and Figure 3.6 show the results of the convergence study for time step and mesh size in the frequency domain respectively.

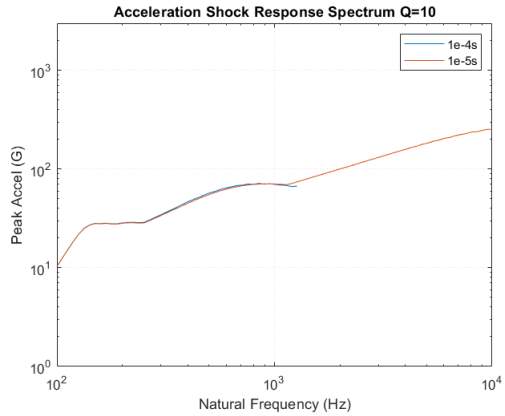

Figure 3.5: Time step Convergence Study for Model with Plate Only for Point (0.2, 0, 0) in the frequency domain.

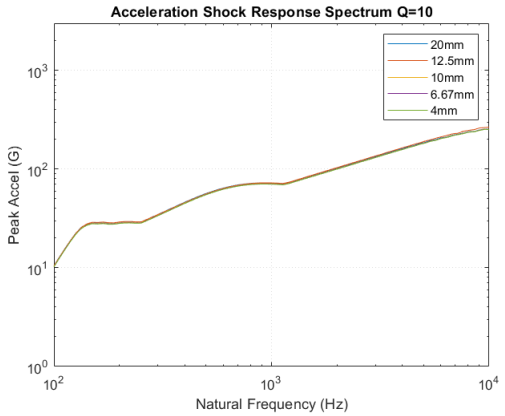

Figure 3.6: Mesh Size Convergence Study for Model with Plate Only for Point (0.2, 0, 0) in the frequency domain.

For the time step, the range of interest spans from 100 Hz to 10000 Hz. The 0.1 ms time step was found to be too large to capture the higher frequencies. As such, the SRS curve using this time step stops just after 1000 Hz, as seen in Figure 3.5. However, it successfully captured the lower-frequency content up to approximately 1000 Hz, showing good agreement with the results obtained using the 0.01 ms time step in this range.

In contrast, the effect of mesh size was significantly smaller in the frequency domain, as seen in Figure 3.6. While slight shifts between the curves were observed, the overall SRS shape and amplitude remained consistent across different mesh densities. This suggests that while mesh refinement is crucial for accurately resolving transient acceleration responses in the time domain, it has a much smaller impact on the frequency-domain representation of the shock event.

The second analysis performed used a similar model to the first one, with the addition of an anvil plate connected to the resonant plate using CBUSH elements, which are one-dimensional spring-damper elements in Nastran that can represent stiffness and damping in all six degrees of freedom between two nodes [27]. The stiffness of these elements was calculated in order to simulate the behaviour of the bolts.

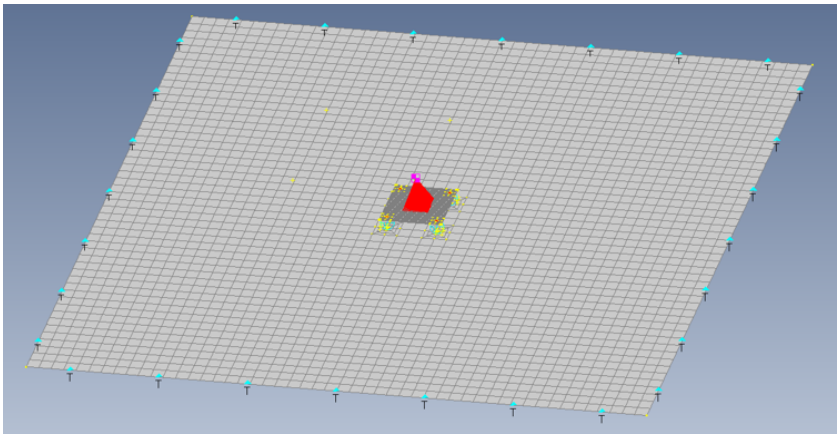

Figure 3.7: Model with RBE2 element connected to anvil plate.

Following the same methodology as before, the study examined the effects of mesh density and time step on the accuracy of the results. The findings, shown in Figure 3.8 and Figure 3.9, are quite similar to those obtained previously with the simpler model.

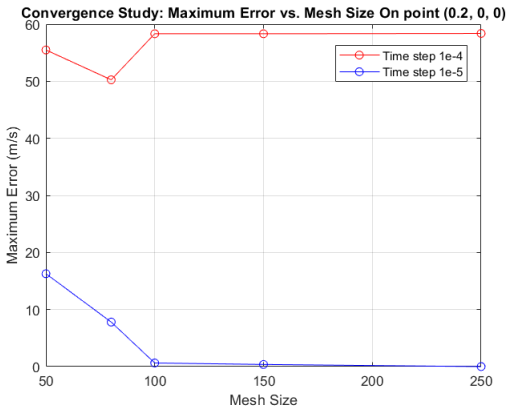

Figure 3.8: Convergence Study for Point (0.2, 0, 0) for Model with Anvil plate and RBE2. Mesh Size is expressed in n x n elements.

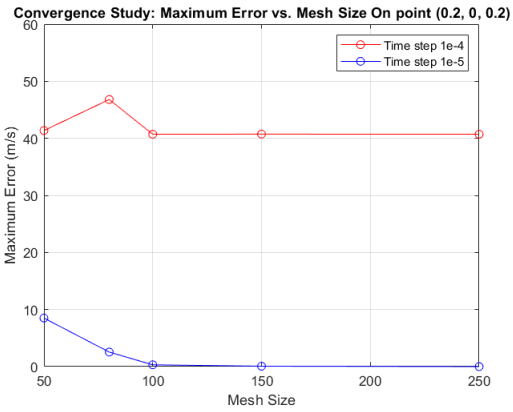

Figure 3.9: Convergence Study for Point (0.2, 0, 0.2) for Model with Anvil plate and RBE2. Mesh Size is expressed in n x n elements.

As seen previously, larger mesh sizes failed to capture the behaviour of higher frequencies, leading to an initial increase in error. However, at a mesh density of 150 by 150 elements, the results converged, with the error approaching zero. This indicates that the inclusion of the anvil plate does not significantly alter the convergence trends observed in the simpler model, further validating the choice of mesh refinement and time step for accurate shock response predictions.

The same study was then repeated in the frequency domain using the Shock Response Spectrum (SRS) method to evaluate the influence of mesh size and time step in this context. Similar to the previous findings, the effect of time step was more pronounced than that of mesh density. Figure 3.10 and Figure 3.11 present these results.

The results in Figure 3.10 confirm that the 0.1 ms time step was too large to capture higher frequencies accurately, with the SRS curve stopping just above 1000 Hz. However, both time steps provided similar results up to this range, as previously observed.

For the mesh density, Figure 3.11 shows that the differences between curves remained small, with only minor shifts in the response. This further supports the conclusion that while mesh refinement is critical for accurate transient acceleration responses, its impact in the frequency domain is less significant, at least for the sizes chosen.

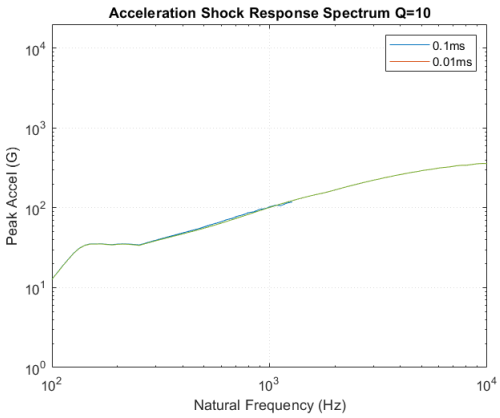

Figure 3.10: Time Step Size Convergence Study for Point (0.2, 0, 0) for Model with Anvil plate and RBE2 in frequency domain.

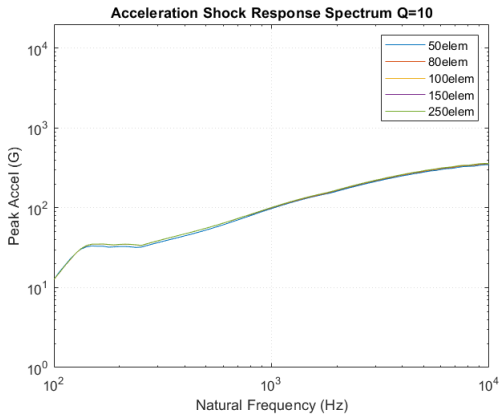

Figure 3.11: Mesh Size Convergence Study for Point (0.2, 0, 0) for Model with Anvil plate and RBE2 in frequency domain. Mesh Size is expressed in n x n elements.

The final iteration of the model included a 50Kg test mass connected to the plate by an RBE2 to evaluate its influence on the accuracy of the results. This addition aimed to assess how an increased mass affects the shock response and the overall convergence behaviour.

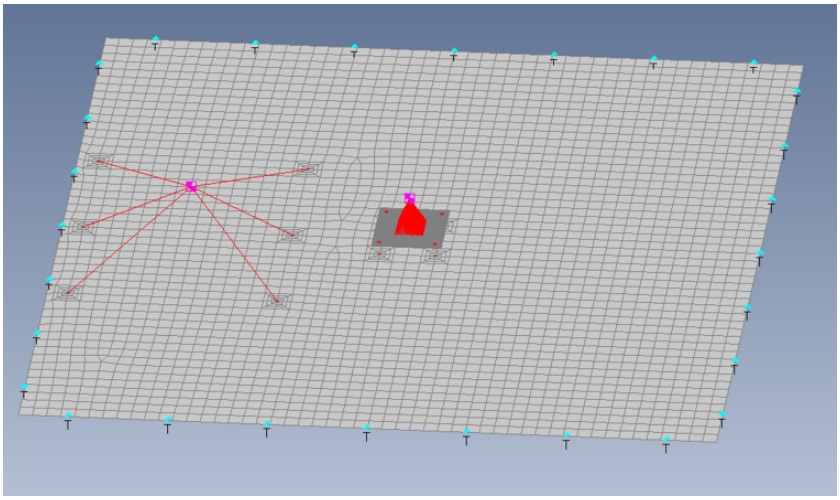

Figure 3.12: Model with RBE2 element connected to an anvil plate with a test mass.

Since the test mass was added on one side of the plate the convergence study in the time domain was made in three different points: (0.2, 0, 0) where the test mass is connected, (0.2, 0, 0.2) and (0, 0, 0.2). Figures 3.13, 3.14 and 3.15 show the errors obtained in the convergence study.

The errors observed are smaller than what was seen previously. The addition of the test mass leads to the significant dampening of the response, which may be responsible for the smaller difference seen between the different mesh sizes used.

The study was also repeated in the frequency domain using the Shock Response Spectrum (SRS) method to analyse the impact of the test mass on the spectral response. The results, shown in Figure 3.16 and Figure 3.17, again demonstrate minimal sensitivity to mesh size, with only slight shifts in the curves, while the time step had a more noticeable effect.

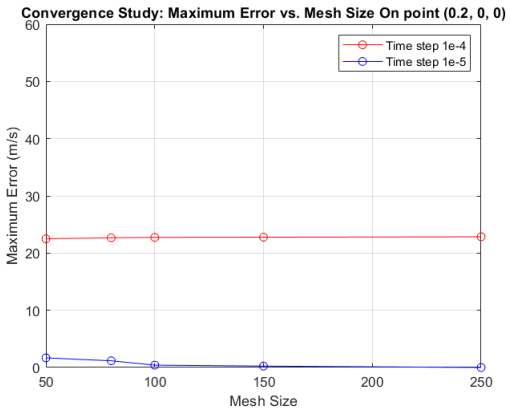

Figure 3.13: Convergence Study for Point (0.2, 0, 0) for Model with Test Mass and RBE2. Mesh Size is expressed in n x n elements.

Figure 3.14: Convergence Study for Point (0.2, 0, 0.2) for Model with Test Mass and RBE2. Mesh Size is expressed in n x n elements.

Figure 3.15: Convergence Study for Point (0, 0, 0.2) for model with Test Mass and RBE2. Mesh Size is expressed in n x n elements.

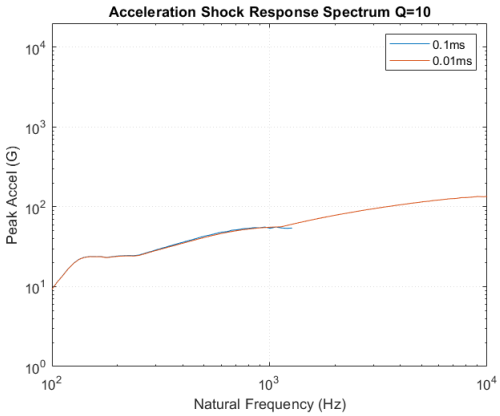

Figure 3.16: Time Step Size Convergence Study for Point (0.2, 0, 0) for Model with Test Mass and RBE2 in frequency domain.

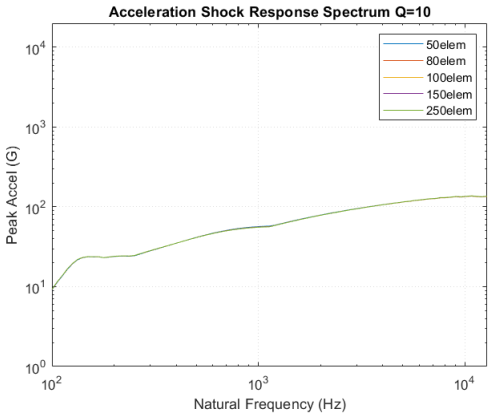

Figure 3.17: Mesh Size Convergence Study for Point (0.2, 0, 0) for Model with Test Mass and RBE2 in frequency domain. Mesh Size is expressed in n x n elements.

As seen in Figure 3.16, the 0.1 ms time step was again insufficient to capture higher frequencies, with the SRS curve terminating just above 1000 Hz. However, both time steps showed strong agreement in the lower-frequency range. Similarly, Figure 3.17 confirms that mesh refinement had a negligible

impact on the frequency-domain results, consistent with previous observations.

These results indicate that while the inclusion of a test mass slightly alters the system dynamics, the overall convergence trends and sensitivity to mesh and time step remain unchanged.

3.2.2. Nonlinear Implicit Transient Analysis

To improve the accuracy of the impact simulation, the second set of models replaces the RBE2-based impact representation with a more realistic approach using linear contact to model the interaction between the hammer and the plate. Unlike the previous models, where the hammer was artificially constrained to remain connected to the plate throughout the simulation, this approach allows for detachment after impact, capturing a more accurate physical response.

This level of detail requires the use of nonlinear implicit transient analysis, which accounts for both the changing contact conditions and the complex material interactions during the impact event. This type of analysis is a time-domain method used to solve dynamic problems where material and geometric nonlinearities, as well as changing boundary conditions, play a significant role [26]. Unlike direct transient analysis, which is typically limited to linear assumptions, this method allows for a more accurate representation of the problem by considering contact interactions, accounting for large deformation, nonlinear material behaviour, and nonlinear wave transmission. In fact, one of the main advantages of this solution type is that it more accurately captures the shock wave throughout the plate, since reflections, mode coupling, and dissipation effects make it a highly nonlinear problem.

Given these advantages, nonlinear implicit transient analysis is well-suited for impact simulations where contact forces evolve over time and where capturing a physically accurate separation between bodies is necessary. However, these benefits come at the cost of significantly higher computational demands compared to linear methods, and they do not eliminate the need for careful fine-tuning. The solution process involves solving large systems of nonlinear equations at each time step, resulting in longer run times and increased memory usage.

Following the same stepwise approach used in the previous set of models, this phase begins with a simplified configuration, where the hammer directly impacts the resonant plate, as shown in Figure 3.18. As in the previous studies, subsequent models increase in complexity by incorporating additional structural elements, such as the anvil and test mass, to assess their influence on the Shock Response Spectrum (SRS).

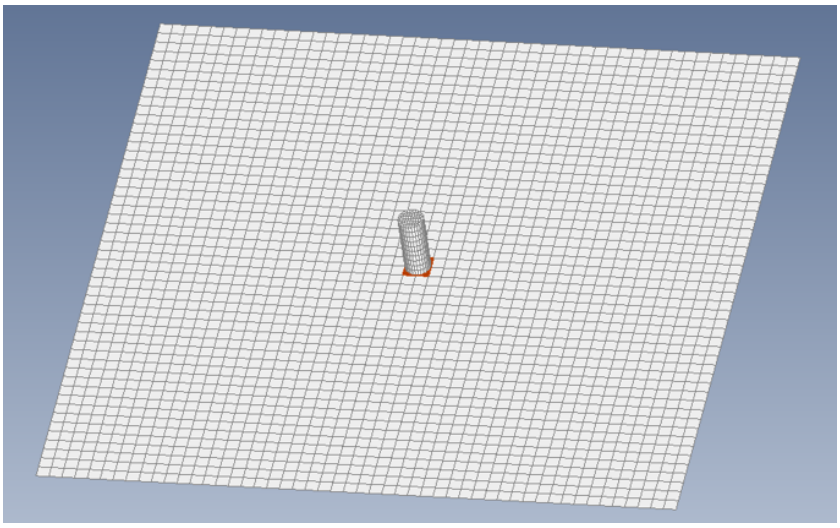

Figure 3.18: Model with only plate and hammer, using linear contact.

It is important to note that, once again, this analysis type does not allow for free moving bodies, so some adjustments were needed to perform the simulation. The resonant plate is pinned at the edges, while the lateral movement of the hammer is constrained, allowing only for vertical movement.

The convergence analysis for the analyses made using the non-linear implicit solution follows the same methodology as before, focusing on evaluating the impact of both time step size and mesh refinement on the results. The results of this first convergence study using the model with only the resonant plate are shown in Figure 3.19 and Figure 3.20.

Figure 3.19 illustrates the influence of mesh refinement by comparing results obtained with different element densities. As observed in the direct transient case, the mesh size has little impact on the computed SRS curves, with all cases displaying strong agreement across the frequency range. However, there still is some small difference in the curves, particularly on the peaks.

The effect of different time step sizes is presented in the Figure 3.20, where it is evident that a larger time step results in an early cut-off of high-frequency content. This occurs because coarser time steps are unable to capture rapid oscillations. The observed trend is consistent with expectations and aligns with the findings from the previous analyses using direct transient analysis. However, while previously the curves matched almost perfectly up until the curve cut-off, in this case, there are some noticeable differences in the responses. The shape at lower frequencies remains similar even if slightly overestimated, but near the cut-off frequency it starts to fail to capture some of the peaks in the response.

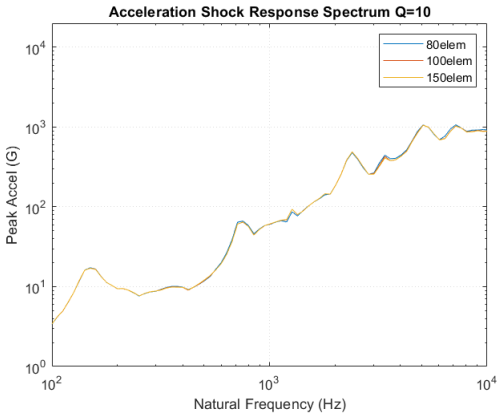

Figure 3.19: Time Step Size Convergence Study for Non-linear Contact Model in Frequency Domain.

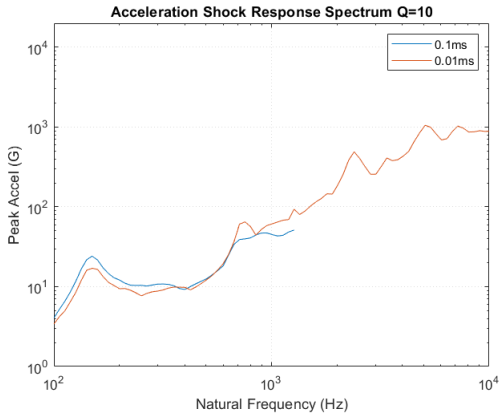

Figure 3.20: Mesh Size Convergence Study for Non-linear Implicit Plate Only Model in Frequency Domain.

3.2.3. Method Comparison

To evaluate the differences between the Direct Transient and Non-linear Implicit Transient analysis methods, the Shock Response Spectrum (SRS) was computed for both cases, as shown in Figure 3.21. This response was the one obtained with the most detailed models, which include the anvil and the test mass. This comparison provides insight into how each approach captures the transient shock response and the extent to which their assumptions impact the final results.

To evaluate the differences between the Direct Transient and Non-linear Implicit Transient analysis methods, the Shock Response Spectrum (SRS) was computed for both cases, as shown in Figure 3.21. This response was obtained using the most detailed models, which include a 50 kg test mass, an aluminium anvil, and a steel hammer with the material properties previously defined in Table 3.4 and Table 3.5. The response was measured at 200 mm from the point of impact, which corresponds to the location of the specimen on the shock table. This comparison provides insight into how each approach captures the transient shock response and highlights the influence of their respective assumptions on the final results.

The SRS results show clear distinctions between the two methods, particularly in the mid-to-high-frequency range. The Direct Transient Analysis, represented by the blue curve, exhibits a smoother and more gradual increase in acceleration with frequency. In contrast, the Non-linear Implicit Analysis, shown in red, predicts significantly higher peak acceleration values at certain frequencies. At low frequencies, below approximately 200 Hz, both methods yield similar results, capturing the first prominent peak of the response. However, the peaks obtained from the Direct Transient Analysis appear more spread out, or ‘elongated,’ over a wider frequency range compared to the clearer, more defined peaks

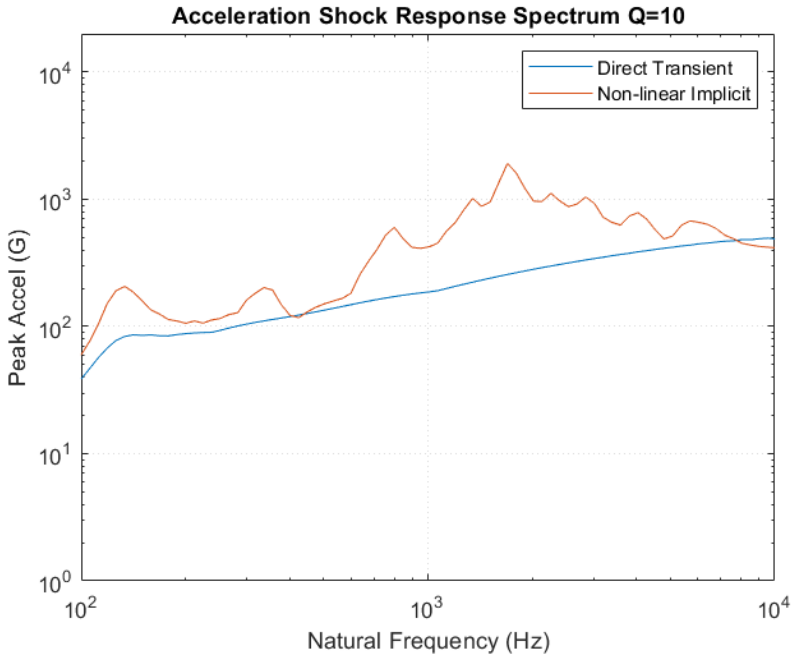

Figure 3.21: Comparison of SRS curves obtained with Direct Transient Analysis and Non-Linear Transient Analysis.

observed in the Non-linear Implicit Analysis. Additionally, the acceleration levels predicted by the Direct Transient Analysis are slightly lower. In the mid-frequency range, between roughly 200 Hz and 1000 Hz, the non-linear Implicit Analysis begins to show oscillatory behaviour with sharper peaks and valleys, whereas the Direct Transient Analysis provides a more uniform response. The difference becomes even more evident at higher frequencies, where the Non-linear Implicit Analysis predicts much higher acceleration peaks compared to the Direct Transient approach, and only aligning again at 10000 Hz.

These discrepancies stem from fundamental differences in how each method handles impact physics, contact interactions, and wave propagation. One of the key factors influencing these results is the way contact is modelled. In the Direct Transient Analysis, the impact is represented using an RBE2 element, which enforces rigid-body motion constraints. This simplification prevents any real separation between the hammer and the plate, which in turn limits the accuracy of the contact force representation. The Non-linear Implicit Analysis, on the other hand, explicitly models contact interactions, allowing for detachment and a more realistic force transmission. As a result, the latter approach introduces stronger high-frequency content, as the force generated during impact is not artificially constrained.

Another important factor is wave propagation and damping. Since the Direct Transient Analysis is by definition linear, it does not fully capture wave reflections and dissipation effects, which leads to an underestimation and/or smoothing out of high-frequency content [25]. In contrast, the Non-linear Implicit Analysis accounts for non-linear effects, including wave reflections, mode coupling, and localised deformations, resulting in stronger oscillations at higher frequencies [26].

These differences highlight important considerations when selecting an analysis approach for shock response studies. The Direct Transient Analysis provides a more computationally efficient solution but may significantly underestimate high-frequency response due to its simplified contact modelling and linear solution. The Non-linear Implicit Transient Analysis captures more realistic impact dynamics, including contact separation and non-linear wave effects, but is computationally more demanding.

3.2.4. Influence of Model Detail on the Shock Response Spectrum

As previously described, for each analysis type used to perform the impact analysis, three models with varying levels of detail were developed: a simplified model consisting of only the plate, an intermediate model where a steel anvil was introduced, and a more detailed model incorporating both the steel anvil and a 50Kg test mass. This section focuses on the assessment of the effect of increasing model

complexity on the shock response spectrum.

The corresponding SRS for these cases using the Direct Transient Analysis are shown in Figure 3.22, illustrating how structural modifications influence the system's dynamic response across different frequency ranges.

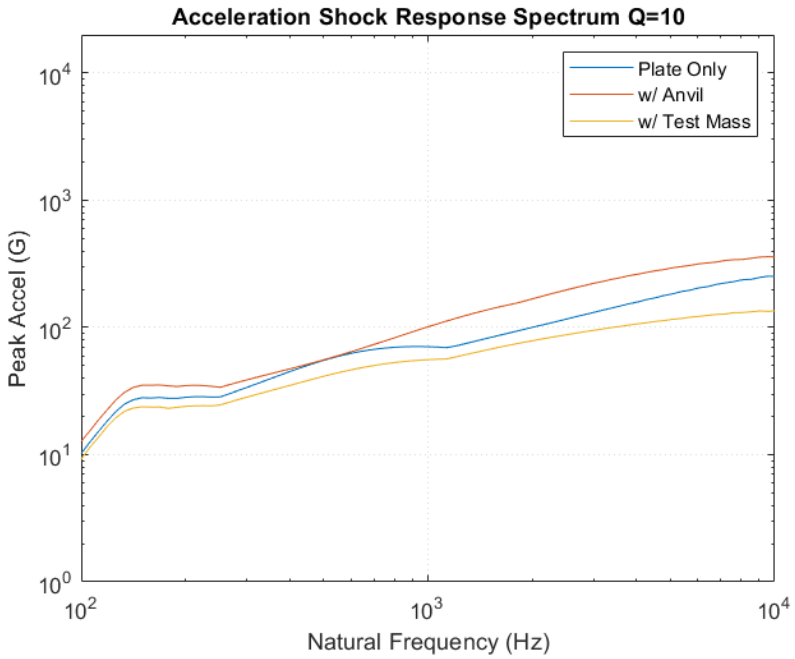

Figure 3.22: SRS Comparison for Models with Varying Levels of Detail using Direct Transient Analysis.

The results indicate that adding more structural elements to the model leads to notable changes in the SRS. At lower frequencies, below approximately 200 Hz, all three models show responses with identical shape, albeit different levels, suggesting that the global system behaviour is primarily dictated by the resonant plate itself. However, as the frequency increases, differences start to emerge. The inclusion of the anvil results in a higher acceleration response across the mid-to-high-frequency range, with a more evident deviation from the plate-only model beyond approximately 1 kHz. This suggests that the anvil enhances the transmission of shock energy, introducing additional structural interactions that amplify certain frequency components.

On the other hand, the introduction of the test mass produces a different effect. While its presence still influences the mid-to-high-frequency response, it notably reduces the peak acceleration values when compared to the plate-only and anvil-included cases. This dampening effect is particularly noticeable above 1 kHz, where the test mass appears to attenuate the high-frequency content of the response. This behaviour likely results from the added inertia and structural coupling effects, which modify the way shock waves propagate through the structure.

For the non-linear implicit case, the resulting SRS curves follow similar trends to those observed in the direct transient analysis but exhibit notable differences due to the inclusion of non-linearity in the solution. The results, shown in Figure 3.23, reinforce the impact of increasing model complexity on the system's dynamic response.

At lower frequencies, all three models display comparable responses, indicating that the global system behaviour remains primarily influenced by the plate itself. Nonetheless, the inclusion of a test mass of 50 kg does result in a noticeable shift to the left in the first peak of the response. As the frequency increases, the differences between the models become more evident. The inclusion of the anvil leads to an increase in acceleration levels at mid-to-high frequencies, similar to what was observed in the direct transient case, further confirming that the anvil contributes to the transmission of shock energy through additional structural interactions. Additionally, at the highest frequency range, this trend is reverted, with the response being more attenuated than with only the plate model.

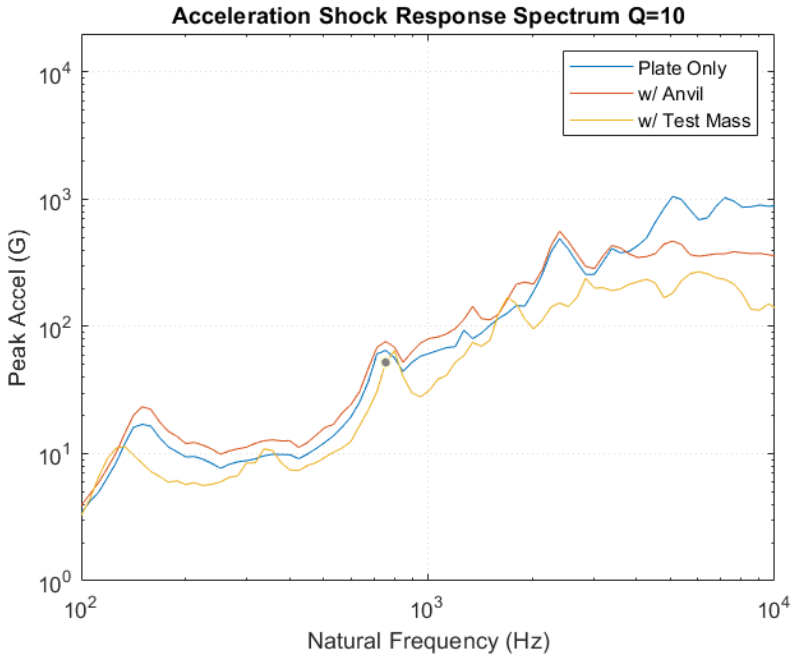

Figure 3.23: SRS Comparison for Models with Varying Levels of Detail using Non-Linear Implicit Transient Analysis.

The presence of the test mass again produces a more significant dampening effect at higher frequencies, reducing peak acceleration values relative to the other models. This attenuation is more pronounced then the previous case using Direct Transient Analysis, particularly beyond 1 kHz, where the test mass significantly lowers the response amplitudes and alters the shape of the peaks. This suggests that in the non-linear regime, the added mass not only alters the structural dynamics but also modifies the way energy is dissipated within the system.

Overall, these results highlight the importance of model detail in capturing the full dynamic response, particularly when non-linearities are considered. The differences between the solutions further reinforce the need to carefully select an appropriate level of detail depending on the specific objectives of the analysis.

3.3. Parameter Study

During a spacecraft's launch, it will be subjected to intense pyroshock loads. Therefore, the launch services provide their costumers with the specific Shock Response Spectrum (SRS) levels that the spacecraft must endure to ensure the spacecraft's structural integrity during the launch process.

These levels have to then be replicated by shock testing facilities as closely as possible within the tolerances defined by the launch provider. However, achieving these levels is a highly complex process, often requiring extensive fine-tuning of the shock table setup and adjustable parameters.

As such, this study of the effect of each individual adjustable parameter is crucial for optimising this fine-tuning process. By investigating the effect of various parameters on the SRS, it becomes possible to better understand how each factor influences the response. This can significantly help reduce the time involved in achieving the desired test levels within the specified tolerances.

Impact Velocity

The impact velocity is one of the easiest parameters to adjust in the design selected for the shock table being developed, as it is driven by the height at which the pendulum hammer is dropped, as shown in Equation 2.4. The simplest model with only the plate was used for this analysis.

Higher impact velocities increase the energy transferred during impact, which is expected to result in a corresponding shift in the Shock Response Spectrum (SRS) curve. The higher the impact velocity, the

more energy is transferred during impact, so it is expected to result in a shift up of the SRS curve. The influence of impact velocity was examined using both analysis methods previously explained: direct transient analysis and implicit nonlinear transient analysis. Figure 3.24 and Figure 3.25 present the results obtained from these methods, respectively.

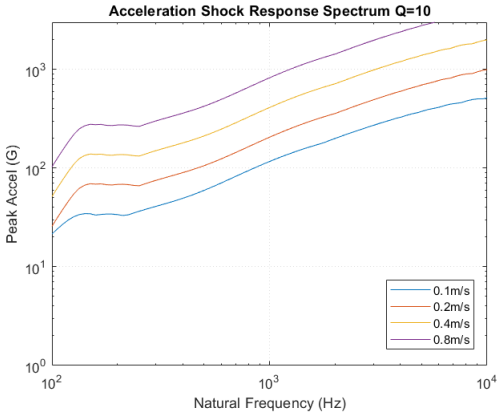

Figure 3.24: Impact Velocity effect on SRS curves, using model with only plate and hammer, using Direct Transient Analysis.

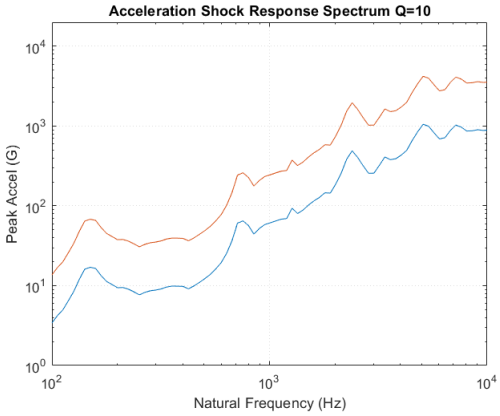

Figure 3.25: Impact Velocity effect on SRS curves, using model with only plate and hammer, using Non-Linear Implicit Transient Analysis.

As seen in both Figures, both analysis methods demonstrate a consistent trend where if the impact velocity increases, the SRS curve uniformly rises across all frequencies. In the cases where Direct Transient Analysis was used, this consisted in a uniform 6dB shift up accross the entire frequency range when doubling the impact velocity. For Non-linear Implicit, only the increase from 1m/s to 4m/s was studied which resulted in a uniform 12dB shift up accross the frequency range, showing that both analysis methods yield identical outcomes. This indicates that higher impact velocities result in a proportional increase in the overall amplitude of the shock response.

Anvil Material

The choice of anvil material is crucial in determining the SRS shape. Different materials for the anvil can significantly alter the response during impact due to their varying mechanical properties, especially their stiffness. The models using the plate and the anvil were used ofr this study.

To study this effect, simulations were performed using three different anvil materials: aluminium 7075, stainless steel and Delrin 150. The first two are metals commonly used in the industry and known for their high stiffness, making them durable and capable of sustaining multiple impacts. The mechanical properties of these materials are shown in Table 3.5. The latter, Delrin 150, was introduced to understand how the response would be affected if the stiffness of the anvil material was significantly reduced. The properties used for Delrin 150 are shown in Table 3.6

Table 3.6: Mechanical Properties of Delrin 150

Property	Value	Unit
Young's Modulus	3.2	GPa
Density	1.41	g/cm^3
Poisson's Ratio	0.35	–

Using both the direct transient and implicit nonlinear transient analysis methods, Figure 3.26 and Figure 3.27 show the differences in SRS due to the material of the anvil.

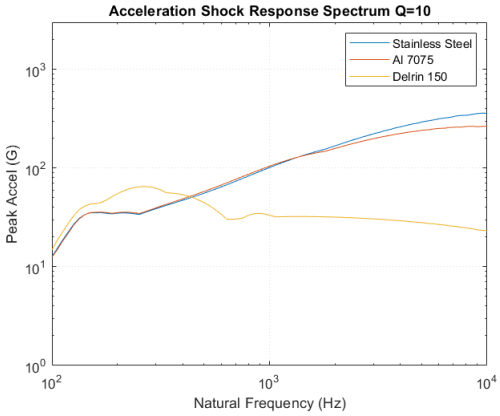

Figure 3.26: Anvil Material effect on SRS curves, using model with plate, anvil and hammer, using Direct Transient Analysis.

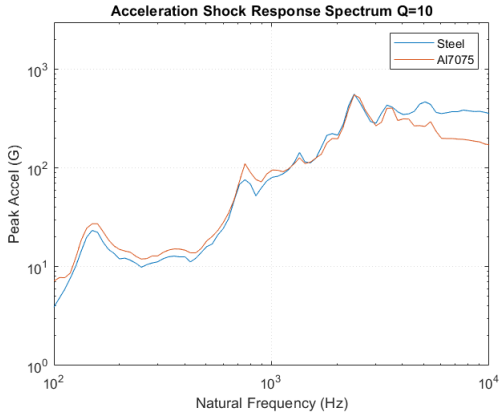

Figure 3.27: Anvil Material effect on SRS curves, using model with plate, anvil and hammer, using Non-Linear Implicit Transient Analysis.

Once again, both analysis methods show consistent behaviour in response to the change. Throughout most of the frequency range, the responses with a stainless steel anvil and an aluminium anvil are nearly identical, with the exception of the high-frequency range. In the case of Direct Transient Analysis, the differences at 100 Hz and 1000 Hz were minimal, with shifts of 0.17 Hz and -0.27 Hz, respectively. The difference only became significant at higher frequencies, reaching an increase of 2.55 dB at 10,000 Hz.

For the Non-linear Implicit Analysis, at 100 Hz, there was a -5.28 dB difference when using a steel anvil compared to an aluminium one. This difference rapidly decreased, and by around 200 Hz, it was less than 1 dB, maintaining this small difference until the mid-frequency range. At higher frequencies, however, the difference became more pronounced, rising to 6.3 dB at 10,000 Hz. Considering these results, the response obtained using the Direct Transient Analysis captures the effect of this parameter on the SRS quite well, despite some minor discrepancies.

These results suggest that the choice of anvil material significantly influences energy dissipation during impact. Harder anvil materials, such as steel, result in higher amplitude responses at higher frequencies due to their greater rigidity, which reduces energy absorption and leads to higher accelerations in the high-frequency range of the SRS curve. In contrast, softer materials like Delrin 150 absorb more energy, resulting in a lower amplitude response and causing the SRS curve to decrease across the majority of the frequency range.

Hammer Mass

The hammer mass is a key parameter to adjust the SRS curve produced by the impact, since by adding or removing mass will lead to more or less kinetic energy being transmitted through the impact. To examine this effect, simulations were conducted using different hammer masses while maintaining all other parameters constant. By systematically varying the mass, the resulting changes in the SRS curve were analysed to determine the influence of this parameter. For this study, the simpler models with only the plate were used.

Using both the direct transient and nonlinear implicit transient analysis methods, Figure 3.28 and Figure 3.29 illustrate the differences in SRS resulting from changes in hammer mass.

Both analysis methods demonstrate a consistent trend in the SRS response due to variations in hammer mass. The results indicate that increasing the hammer mass leads to a higher response across the entire SRS curve. However, this upward shift is more pronounced in the lower frequency spectrum. Using the Direct Transient Analysis, increasing the hammer mass from 2 kg to 4 kg resulted in increases of 10.24 dB, 5.37 dB, and 3.2 dB at 100 Hz, 1000 Hz, and 10,000 Hz, respectively. When the mass was increased from 4 kg to 10 kg, the increases were 4.22 dB, 2.88 dB, and 2.11 dB at 100 Hz, 1000 Hz, and 10,000 Hz, respectively.

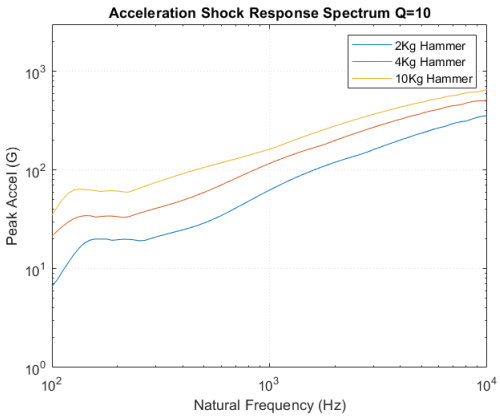

Figure 3.28: Hammer mass effect on SRS curves, using model with plate only, and hammer, using Direct Transient Analysis.

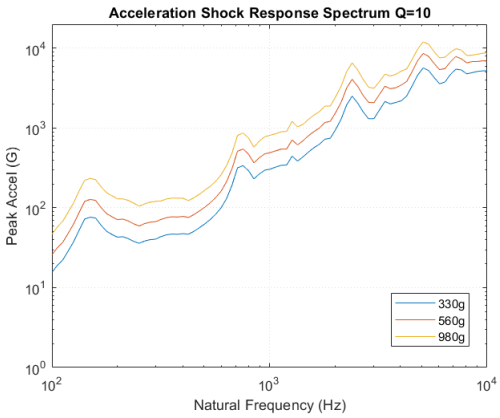

Figure 3.29: Hammer mass effect on SRS curves, using model with plate only, and hammer, using Non-Linear Implicit Transient Analysis.

For the Non-Linear Implicit Analysis, the increase in mass followed a constant trend, with a 1.7 times increase in mass resulting in increases of 4.40 dB, 4.13 dB, and 2.3 dB at 100 Hz, 1000 Hz, and 10,000 Hz, respectively. This behaviour occurs because the impact generates a stronger excitation at lower frequencies, while higher frequencies are more influenced by material stiffness and contact dynamics, rather than mass alone.

Once again, the Direct Transient Analysis was able to capture the overall behaviour of this parameter change, accurately reflecting the trend observed in the results despite some minor discrepancies.

Hammer Material

The simplified models using a point mass connected to the plate with an RBE2 using direct transient analysis can not be used for this study as it is not possible to specify the hammer material. Once again, the simplest models with only the aluminium plate were used.

To study the impact of different hammer materials, simulations were performed using two materials: stainless steel and titanium. These materials are commonly used for impact hammers in shock testing facilities due to their durability and rigidity.

Initially, this study involved directly altering the material properties of the modelled hammer, which not only affected its rigidity but also its mass.

To isolate the effect of material stiffness, the model was later adjusted to ensure that the mass of the hammer remained identical for both materials. This modification allowed the study to focus solely on the impact of material stiffness without the influence of mass variation.

Figure 3.30 presents the differences in the SRS due to the material of the hammer.

The simulations show that both materials produce very similar SRS curves. While the use of a harder material such as stainless steel leads to a slightly higher amplitude response across the frequency range, particularly at higher frequencies, this effect is minimal. The increased response is attributed to the greater rigidity of stainless steel, which results in reduced energy absorption and consequently higher accelerations during impact. However, due to the similarity in Young's Modulus between the materials, the overall difference remains negligible, with variations of less than 1 dB observed across all frequencies.

Test Specimen Mass

The mass of the test specimen is a crucial parameter that significantly influences the shock response during testing. To understand its impact, simulations were conducted with different test masses: 12.5 kg, 25 kg, 50 kg, and without any test mass for comparison. These variations simulate different specimen weights that might be encountered in shock testing.

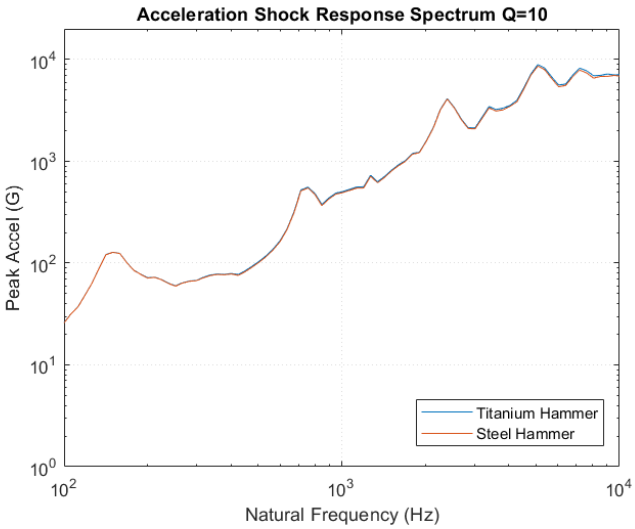

Figure 3.30: Hammer material effect on SRS curves, using model with plate only, and hammer, using Non-Linear Implicit Transient Analysis.

The models used for this study consisted of the plate with an aluminium anvil and a titanium hammer plus the varying test mass. As shown in Figure 3.31 and Figure 3.32, the changes in the SRS resulting from these varying test masses were analysed.

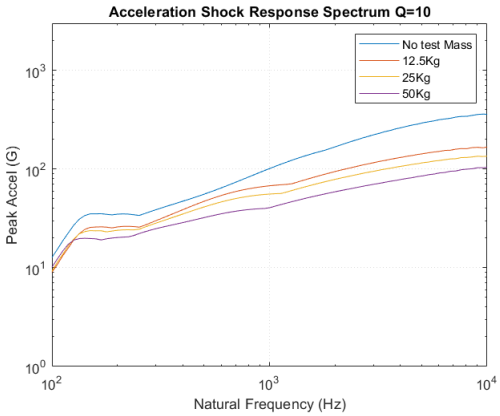

Figure 3.31: Test Specimen Mass effect on SRS curves, using model with plate, anvil, hammer, and test mass, using Direct Transient Analysis.

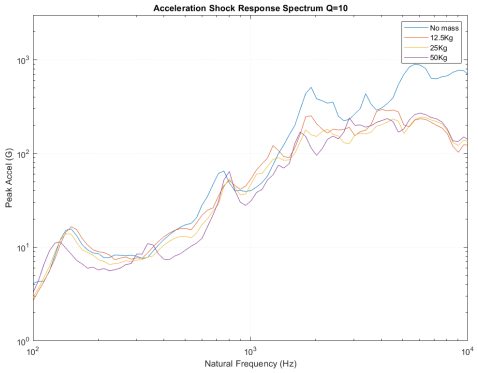

Figure 3.32: Test Specimen Mass effect on SRS curves, using model with plate, anvil, hammer, and test mass, using Non-Linear Implicit Transient Analysis.

With the addition of the 12.5 kg test mass, the SRS response notably shifts downwards, particularly in the higher frequency ranges. Direct Transient Analysis (DT) showed differences of 3.31 dB, 3.48 dB, and 9.27 dB at 100 Hz, 1000 Hz, and 10,000 Hz, respectively. The Non-Linear Implicit (NL Implicit) analysis yielded differences of 2.99 dB, 3.54 dB, and 6.56 dB at these frequencies. These results demonstrate that the addition of a test mass leads to the decrease of the SRS curve, with the largest reduction occurring in the higher frequencies. Notably, Direct Transient Analysis effectively predicted the influence of this parameter on the SRS response, capturing the overall trend observed.

When the test mass increased from 12.5 kg to 25 kg, the differences observed using NL Implicit were 0.79 dB, 1.12 dB, and 0.71 dB at 100 Hz, 1000 Hz, and 10,000 Hz, respectively. For DT, the differences were 0.21 dB, 1.68 dB, and 1.88 dB at these same frequencies. These results indicate that as the test mass continues to increase, the SRS curve keeps shifting downward, with the most significant decrease occurring in the mid-frequency range. Again, Direct Transient Analysis captured the overall behaviour of the parameter change, providing a good match to the observed results.

Further increasing the mass from 25 kg to 50 kg, NL Implicit analysis showed differences of 0.96 dB, 3.60 dB, and 0.33 dB at 100 Hz, 1000 Hz, and 10,000 Hz, respectively, while DT produced differences of 0.81 dB, 2.74 dB, and 2.26 dB at these frequencies. This continuation of the trend further highlights that the SRS curve keeps decreasing, with the mid-frequency range again showing the largest decrease. As before, the Direct Transient Analysis predicted the parameter influence on the SRS well, capturing the general trend of reduced amplitudes across all frequencies.

In all cases, the inclusion of a heavier test mass absorbs more energy during the impact, leading to reduced acceleration amplitudes, particularly in the mid- and high-frequency ranges. The SRS curve shows a significant reduction in amplitude as the test mass increases, as the added mass dissipates more energy. Additionally, there is a slight shift to the left in the peaks observed in the responses as the test mass increases, indicating a change in the frequency characteristics of the system due to the added mass.

Measurement Location

While the test specimen position remained constant in the shock table design, a study was conducted to assess how the SRS curve varies depending on the measurement location on the plate, in order to better understand how the shock propagates through the structure. This study was conducted using the simplest models with only the aluminium plate.

For the Direct Transient Analysis, two measurement points were considered: point one located 0.2 m directly from the point of impact, and point 2 located 0.2 m diagonally from the impact point (i.e., towards a plate corner, representing a lateral offset). In the Non-Linear Implicit Analysis, an additional third point was included at 0.4 m directly away from the impact point, extending the range of the investigation. **??** shows the postioning of these points in the plate.

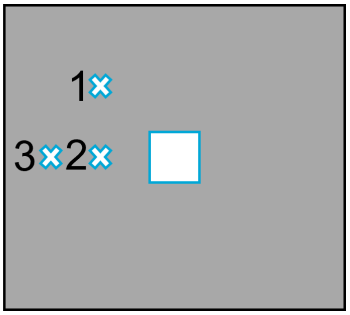

Figure 3.33: MEasurement Locations on the plate.

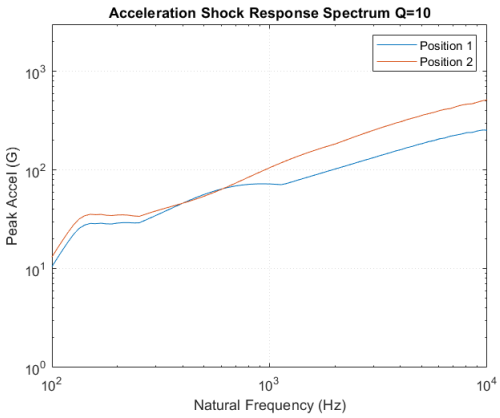

Figure 3.34: Measurement location effect on SRS curves, using model with plate only, using Non-Linear Implicit Transient Analysis.

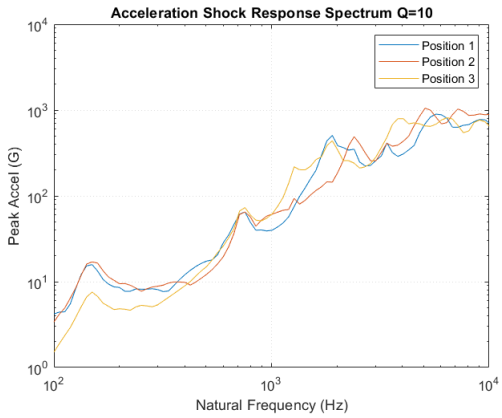

Figure 3.35: Measurement location effect on SRS curves, using model with plate only, using Non-Linear Implicit Transient Analysis.

As shown in Figure 3.34 and Figure 3.35, the SRS responses vary depending on the measurement

location. Although more data would be required for definitive conclusions, preliminary results indicate that as the measurement point moves further from the impact location, the SRS amplitude tends to decrease. This suggests that energy dissipates as it travels through the plate.

Moreover, the appearance of peaks at different frequencies depending on the measurement location suggests sensitivity to local mode shapes. This implies that the frequency content of the response is influenced by the structural dynamics at each specific location on the plate. While the test specimen position is constant, a study was performed by analysing the SRS curve obtained at different locations on the plate to better understand how the shock propagates through the plate.

4

Design Space Exploration through SRS curve Matching

Shock testing facilities are designed to replicate the Shock Response Spectrum (SRS) levels provided by launch providers, ensuring that spacecraft and their components can withstand the dynamic loads experienced during launch and throughout their mission. Achieving the required SRS levels within the specified tolerances is a complex process, which requires significant fine-tuning of the shock table setup and careful selection of key parameters. Thus, this process involves iterative adjustments in order to align the simulated response with the desired SRS curve.

In this study, due to the iterative nature of SRS matching, this is approached as a design space exploration process rather than a purely validation-oriented analysis. By systematically varying key parameters such as impact velocity and hammer and anvil physical properties, it is possible to assess how they affect the system's dynamic response, providing valuable insight into the optimal shock table setup required to achieve the desired SRS.

For this chapter, only the detailed models employing non-linear implicit transient analysis were used, as these simulations provide the most accurate representation of the physical phenomena involved. These models simulate the impact using contacts, allowing for a more realistic evaluation of the parameter adjustments necessary to achieve the target SRS curve. The insights gained from these simulations inform the design and setup of the physical shock table, ensuring that the final configuration is based on a well-characterised parameter space.

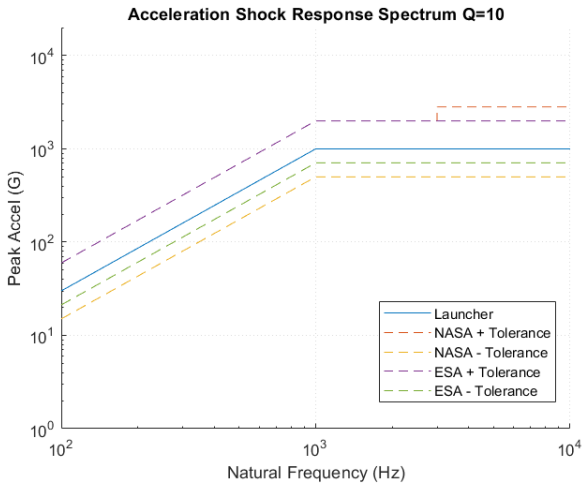

Figure 4.1: Target SRS, including tolerances [5][6][7].

For this study, the target SRS values are derived from the specifications of the Falcon 9 launch vehicle, which defines the expected acceleration response across a range of frequencies [5]. Figure 4.1 presents the target SRS levels, including the acceptable tolerance range. This tolerance band accounts for variations in shock responses due to different test setups and material properties, while ensuring compliance with launch provider requirements.

As previously mentioned, achieving these target levels requires careful selection of impact parameters and iterative fine-tuning of the simulation setup. The following sections describe the methodology used to refine the simulated SRS and align it with the specified target.

4.1. Methodology for Achieving the Target SRS

The methodology for achieving the target SRS involves a systematic approach in which the simulation results are iteratively refined to match the specified curve. Through the use of non-linear implicit transient analysis, the process simulates the shock event, adjusting parameters, and assessing results until the SRS response matches the target within the specified tolerances. Below is a description of the key steps involved:

1. **Identify Key Parameters**
   The first step is to determine the parameters that influence the SRS response without requiring major design modifications. Based on previous studies and analyses in section 3.3, impact velocity, impactor mass and material, and anvil material were identified as the most effective variables to adjust the response. These parameters directly affect the energy transfer and frequency distribution of the shock event.

   To establish a reference point, an initial **base model** was created using reasonable selections for these parameters. This model serves as a baseline for future iterations, allowing systematic adjustments to better match the target SRS.

2. **Perform Simulation and Obtain Acceleration Time History**
   In this step, after selecting the parameters, the shock impact is simulated by running the non-linear implicit transient analysis. Once the simulation is completed, the next task is to extract the acceleration time history from the location where the accelerometer would be positioned near the test specimen. This time history represents the table's dynamic response and is crucial for evaluating the shock environment during the test.

3. **Transform Acceleration Time History to SRS**
   Once the acceleration time history is obtained, the next phase involves calculating the Shock Response Spectrum (SRS) based on this data. To do this, a MATLAB code developed by Professor Tom Irvine was used [28]. This code, available publicly, was modified to suit the specific requirements of this study. The code processes the acceleration time history and calculates the shock response across various frequencies, ultimately generating the SRS curve. This transformation is critical to compare the shock table's performance to the target SRS.

4. **Analyse Results and Refine Parameters**
   After obtaining the SRS curve from the simulation, the next critical task is to compare the simulated SRS with the target SRS curve. This comparison helps identify any discrepancies in key features such as peak acceleration levels, frequency responses, or overall shape of the curve. In this phase, we focus on the areas where the simulated response deviates from the target, noting specific frequencies or regions that require refinement.

   Based on this analysis, adjustments are made to the shock table parameters to improve the match between the simulated SRS and the target. Each change is implemented systematically, and the simulations are rerun after each adjustment to evaluate the impact of the modification on the SRS. This process of comparing results and tweaking parameters is iterative, ensuring continuous refinement of the shock table setup.

Once the simulated SRS aligns with the target SRS within the specified tolerances, the process is considered complete.

4.2. Model Description

A finite element model (FEM) was created to simulate the shock impact event using nonlinear implicit transient analysis. This analysis method was chosen for its ability to model complex interactions during impact, including contact between the various components of the shock table and the test specimen. The nonlinear nature of the model accounts for the material deformations and energy transfer involved in the shock event.

The model consists of several components:

- A 1m x 1m x 3cm aluminium plate representing the shock table surface.
- An anvil plate, which can be modelled in either aluminium or steel depending on the setup.
- A hammer, which can be made of either titanium or steel. The mass of the hammer can be adjusted by adding weight, allowing for flexibility in simulating different impact forces.
- A test specimen, which is modelled as a mass element connected to the shock table plate via an RBE2 (Rigid Body Element).

Two different test specimen masses were considered for the simulations: one at 50 kg and the other at 25 kg. The process of achieving the target SRS was performed separately for each specimen mass, with the goal of replicating the shock environment for both test conditions.

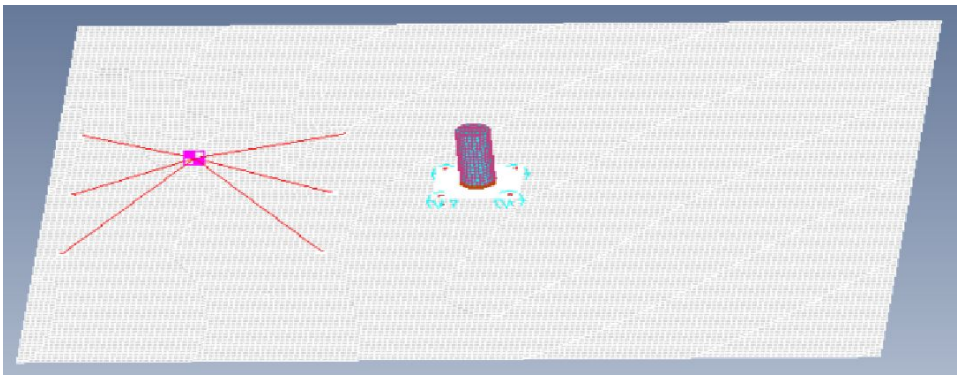

Figure 4.2: Model with Test Mass.

Due to the limitations of the analysis method used, some boundary conditions had to be applied to the model. The plate was pinned in place, as the analysis type used does not allow for free-floating elements. This ensures that the plate remains stationary during the shock impact simulation. The hammer was also constrained in lateral movement, with only vertical movement allowed. This constraint reflects the physical limitation of the analysis method but is consistent with how the shock table operates in reality, where lateral movement is minimal during impact.

4.3. Design Space for 50 kg Test Specimen

With the finite element model established and the key parameters identified, the next step is to achieve the target Shock Response Spectrum (SRS) for the 50 kg test specimen. This section presents the methodology used to refine the shock table parameters and simulate the shock environment in order to match the Falcon 9 launch vehicle's SRS requirements. The process follows the steps outlined earlier, with adjustments made iteratively to achieve the desired match.

The initial simulation for the 50 kg test specimen used a steel anvil, a titanium hammer, and an impact velocity of 0.5 m/s. These base parameters were selected based on prior research and the specifications provided by the Falcon 9 launch vehicle. The first simulation was conducted with these values, and the acceleration time history at the location near the test specimen was recorded.

Figure 4.3 presents a comparison between the SRS obtained with the first simulation attempt and the target.

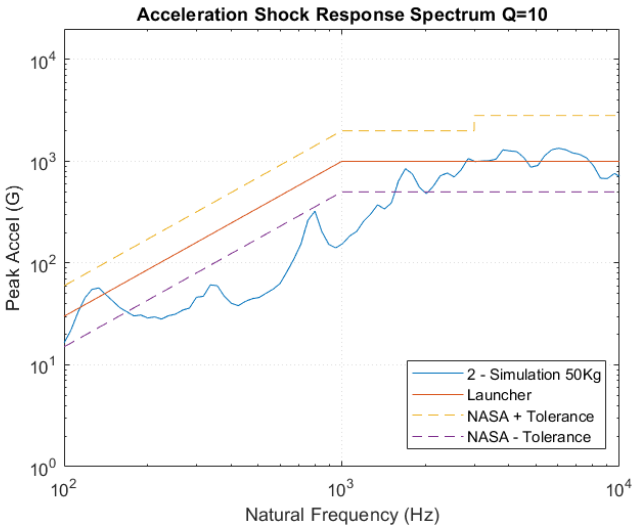

Figure 4.3: Comparison between SRS obtained in first simulation vs Target.

Upon analysing the results, it was observed that the simulated SRS closely matched the target SRS at higher frequencies, indicating that the system was able to produce the necessary response in the high-frequency range. However, in the lower frequency range, particularly below the knee frequency of the target curve, the simulated SRS was still below the desired levels. This indicated that adjustments were needed to increase the low-frequency response of the shock table.

Given the observed discrepancies in the low-frequency range, the next step was then to refine the parameters to improve the match. Therefore, for the second iteration, the material of the hammer was changed from titanium to steel. Since steel has a higher density, this will lead to an increase at lower frequencies compared to the titanium hammer, making them more suitable for achieving the desired low-frequency response.

Figure 4.4 presents a comparison between the SRS obtained with the second simulation attempt and the target. Comparing the results with the first simulation reveals that this modification successfully increased the response in the low-frequency range, below the knee-frequency, bringing it closer to the lower tolerance limit. The high-frequency response remained mostly unchanged, confirming that the adjustment did not negatively impact that region. However, despite this improvement, the results still do not fully fall within the required tolerances, indicating that further refinements are necessary.

Since the higher frequencies were already mostly in line with the desired curve, it was feared that additional changes made in the parameters in order to increase the response in the lower frequency range would lead to over-testing at higher frequencies. Therefore, the following simulations used an aluminium anvil to prevent this from happening.

For the sake of brevity, not all iterations performed during the parameter tuning process will be described in detail, nor will all results be presented. Instead, only the most relevant attempts and key decisions will be highlighted, focusing on the rationale behind the changes made and their impact on achieving the target SRS.

As expected, the iteration with the aluminium anvil successfully lowered the response in the higher frequency range while leaving the lower frequencies largely unchanged, as shown in Figure 4.5. However, while this modification prevented excessive high-frequency content, it also resulted in a slight reduction of the response at these frequencies, bringing them just below the lower tolerance limit for frequencies close to 10000 Hz. Additionally, the levels below the knee frequency remained insufficient, since the adjustment was not meant to address this issue. To compensate for the lower levels, the impact velocity was increased in the following iteration in an attempt to raise the overall response across all frequencies. This adjustments raises the levels uniformly across the entire frequency range, and it was deemed not enough since to be able to fit the lower frequency range levels within the tolerances,

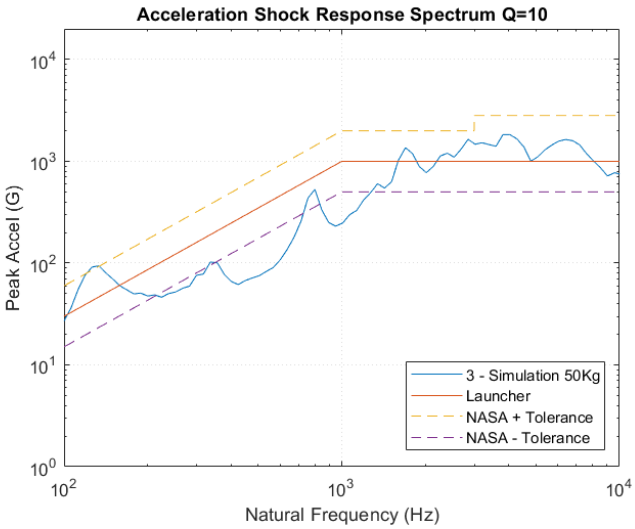

Figure 4.4: Comparison between SRS obtained in second simulation vs Target.

it was required to significantly over-test the test mass in the higher frequency range.

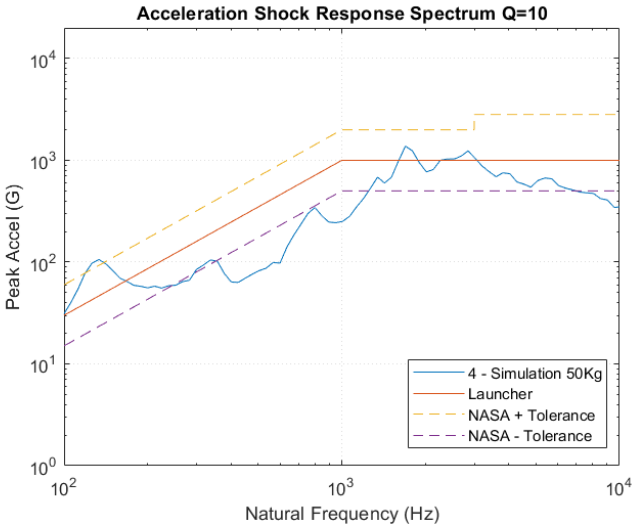

Figure 4.5: Comparison between SRS obtained in fourth simulation vs Target.

Therefore, the next step was to increase the hammer mass, as both prior studies and literature indicated that a heavier hammer has a stronger influence on this frequency range. Figure 4.6 presents the results after this change. The increase in hammer mass successfully raised the response in the lower frequency range, bringing it closer to the target curve, with only a slight drop below the lower tolerance limit between 400 Hz and 600 Hz. However, this adjustment also led to an over-excitation of a plate mode at 130 Hz, resulting in slight over-testing at this frequency. Additionally, the response at higher frequencies, particularly near 10,000 Hz, remained slightly below the lower tolerance limit.

While there are still minor discrepancies, the results showed a significantly improved match, particularly in the problematic low-frequency region. Therefore, the following iterations consisted of adjusting the impact velocity and the hammer mass until the response fell within the tolerance limits.

Once a satisfactory match was achieved using the non-linear implicit transient approach, a final comparison was conducted to assess how well this method predicted the shock response relative to an alternative direct transient solution. This evaluation is essential to determine the practicality of using the direct transient method, which requires significantly lower computational resources.

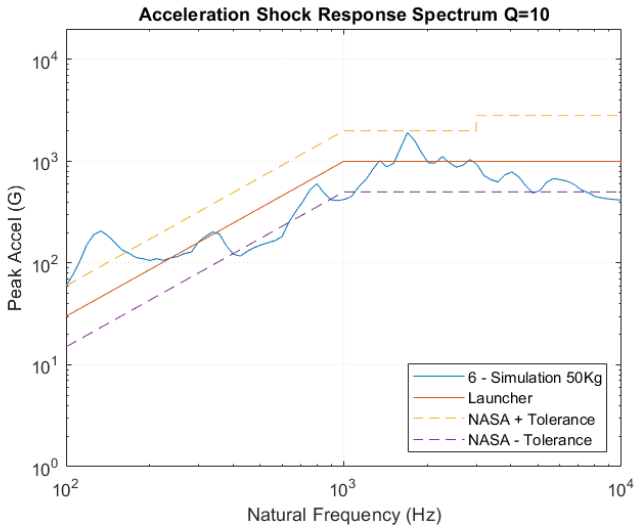

Figure 4.6: Comparison between SRS obtained in sixth simulation vs Target.

For a fair comparison, the direct transient simulation was set up as closely as possible to the final nonlinear implicit model. In this case, the 50 kg test specimen setup included a 10 cm thick aluminium anvil impacted at 0.8 m/s. Although most parameters were kept consistent, minor adjustments were necessary due to differences in how each solver handles contact interactions and numerical integration. Since explicit solvers do not model contacts in the same way, the impact was simulated using a mass element representing the hammer's weight, connected to the anvil by an RBE2 element. In Figure 4.7, a comparison of the SRS results obtained from both methods against the target levels is presented.

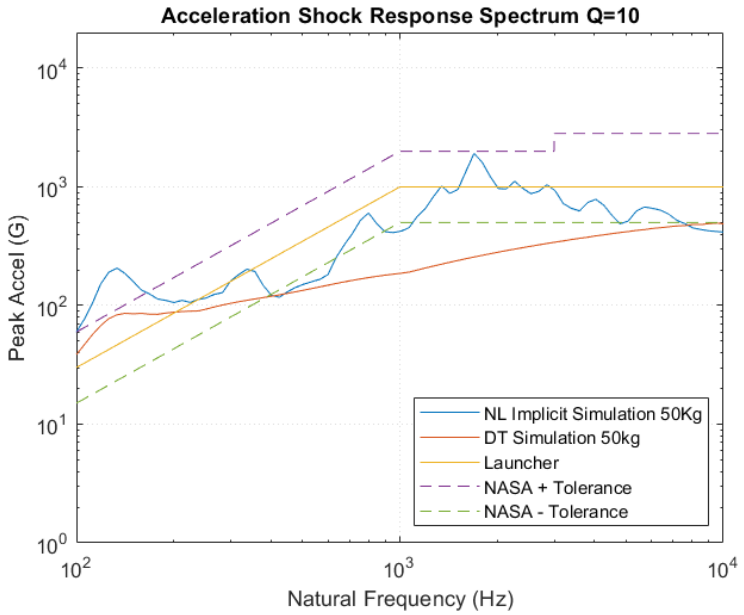

Figure 4.7: Comparison between final Nonlinear Implicit and Direct Transient simulation results for the 50 kg test specimen.

The comparison reveals that both the nonlinear implicit and direct transient methods capture the overall SRS trend, particularly in the low-frequency region and the high-frequency plateau. However, a key distinction is that the direct transient simulation consistently underpredicts acceleration levels across the entire frequency spectrum.

At lower frequencies, both methods capture the initial peak, indicating that they adequately model the dominant low-frequency behaviour. However, beyond this point, the direct transient solution produces

a notably smoother response, with fewer secondary peaks compared to the nonlinear implicit approach. This suggests that the direct transient solver may be less sensitive to localised resonances, likely due to its linearised treatment of contact and damping effects.

Ultimately, this comparison underscores the trade-off between computational efficiency and solution accuracy. While the direct transient method remains a practical starting point, particularly for early-stage design iterations, the nonlinear implicit approach provides a more refined representation of the shock response, making it the preferred choice for final validation.

4.4. Design Space 25 kg Test Specimen

The objective of this section is to explain how the target Shock Response Spectrum (SRS) was achieved for the 25 kg test specimen. Since the 25 kg specimen is lighter than the 50 kg specimen, it was anticipated that the shock response would behave differently, especially in terms of the low-frequency response. Therefore, the initial parameters for this simulation were carefully selected based not only on the literature study but also on the findings from the 50 kg case.

For the initial simulation of the 25 kg test specimen, the following parameters were chosen: an aluminium anvil, a steel hammer, and an impact velocity of 0.6 m/s. These choices were based on the observations from the 50 kg test specimen simulation, where adjustments in hammer material and impact velocity were considered essential to achieving a better match with the target SRS.

The first simulation was run with these parameters and the resulting acceleration time history was extracted. This time history was used to calculate the simulated SRS using the same process as before. The simulated SRS was then compared to the target SRS for the Falcon 9 launch vehicle, as shown in Figure 4.8.

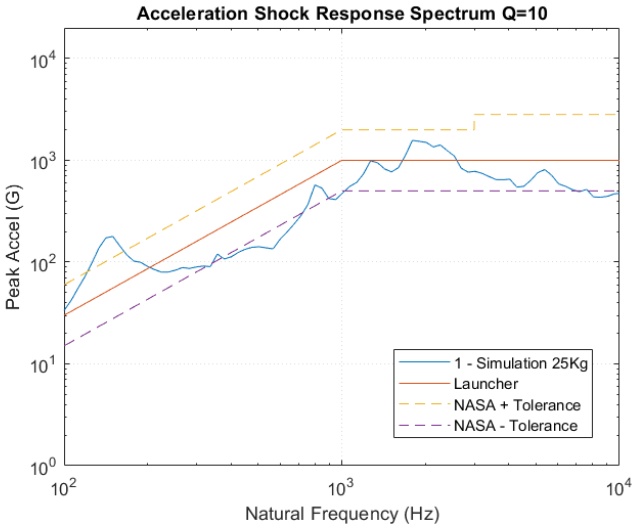

Figure 4.8: Comparison between SRS obtained in first simulation vs Target.

Examining the graph, it is evident that the simulated response already aligns more closely with the target SRS than the first iteration of the 50 kg case. This improvement can be attributed to the more informed selection of initial parameters. However, discrepancies remain, particularly in the region just below the knee frequency, where the response is lower than desired. Additionally, the higher frequency range does not yet reach the upper tolerance limits, indicating that further tuning is required.

To address these issues, modifications were made in the next iteration. Specifically, the anvil material was changed from aluminium to steel to provide a stiffer impact surface, and the impact velocity was increased to 0.7 m/s to raise the overall response. The results of these adjustments are presented in Figure 4.9.

For the second simulation, two changes were made in the parameters to address these critical zones. The anvil was changed to steel and the impact velocity was increased to 0.7 m/s. The results of these

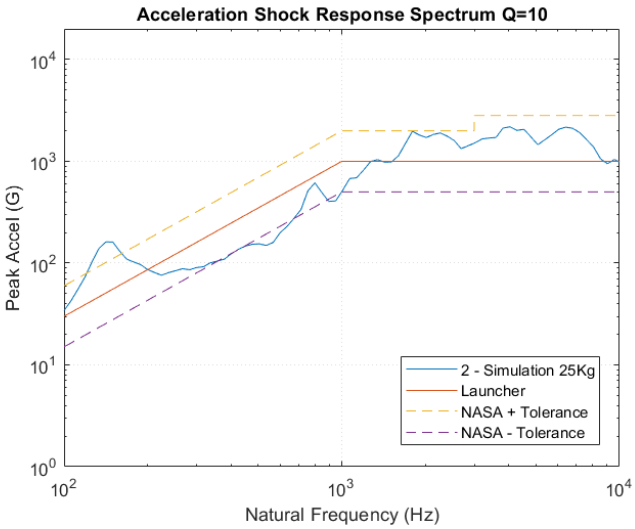

Figure 4.9: Comparison between SRS obtained in second simulation vs Target.

changes are shown in Figure 4.9.

As seen in the updated SRS, the higher frequency range now falls within the tolerance limits, confirming that the increased impact velocity effectively boosted the response in this region. However, despite some improvement, the response just below the knee frequency remains slightly below the lower tolerance boundary.

To further enhance the low-frequency response, two additional changes were made. First, the hammer mass was increased by 50%, as both prior studies and literature indicated that hammer mass predominantly affects the lower frequency range. The results of these changes are presented in Figure 4.10.

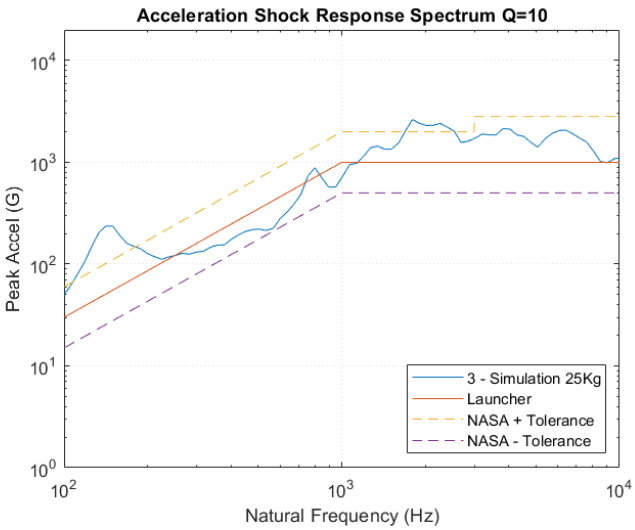

Figure 4.10: Comparison between SRS obtained in third simulation vs Target.

The results obtained from this third iteration demonstrate that the response now remains within the tolerance limits across all frequencies, ensuring that no part of the curve falls below the lower boundary. However, this adjustment also led to an over-excitation of a plate mode at approximately 130 Hz, resulting in noticeable over-testing at this frequency. A similar effect was observed just below 3000 Hz, although in this case, the deviation was minor and considered acceptable for the current study.

After refining the shock table setup and achieving a satisfactory match with the target SRS using the

nonlinear implicit transient approach, an additional comparison was conducted to evaluate how well this method predicts the shock response relative to an alternative direct transient (DT) simulation. This step is particularly important, as the Direct Transient solution requires significantly less computational effort, making it a potentially more efficient alternative.

To ensure a fair comparison, the Direct Transient simulation was performed using a setup as similar to the final nonlinear implicit model as possible. Specifically, a 10 cm thick steel anvil was impacted at 0.7 m/s, mirroring the conditions used in the nonlinear implicit case. However, due to fundamental differences in solver capabilities, certain modifications were necessary, specifically in how the impact was modelled. Since contact definitions are not available in the Direct Transient approach, the hammer's effect was simulated using a mass element with the same weight as the hammer, connected to the anvil via an RBE2 rigid body element. The results of this comparison are shown in Figure 4.11, where the SRS curves obtained from both methods are plotted alongside the target launcher levels.

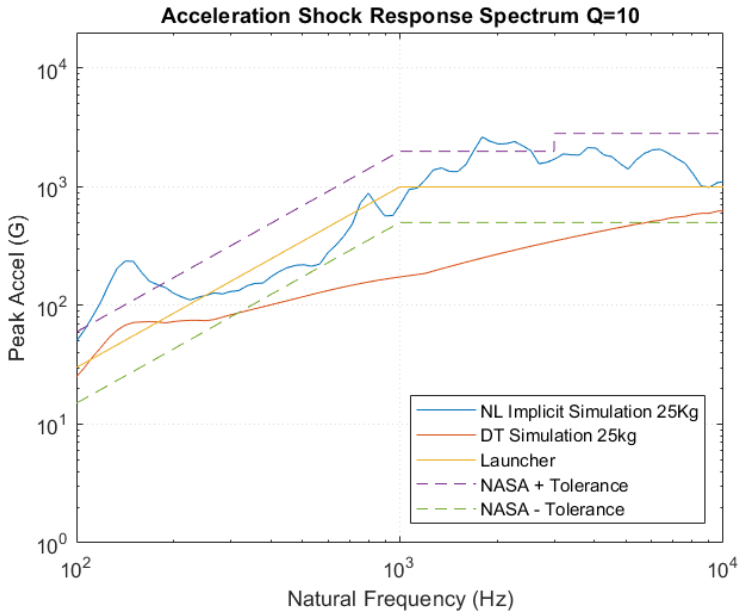

Figure 4.11: Comparison between final Nonlinear Implicit and Direct Transient simulation results.

An analysis of the graph reveals that while both methods produce SRS curves with similar overall trends, there are notable differences in their predicted levels. The most significant discrepancy is that the direct transient solution consistently underestimates the response across the entire frequency spectrum.

In the low-frequency range, both methods capture the first peak with similar shapes, indicating that they adequately model the dominant low-frequency behaviour. However, beyond this region, the direct transient solution produces a noticeably smoother response with fewer peaks. This reduced fluctuation is likely due to the linearised approach of the direct transient solver, which inherently simplifies the representation of a highly non-linear impact event.

While both methods provide a reasonable approximation of the target SRS, the observed differences underscore the importance of solver selection in accurately predicting shock responses. The non-linear implicit approach, despite its higher computational cost, offers a more detailed and realistic representation of dynamic interactions, making it the preferred choice for refining shock table configurations. However, the direct transient method remains a useful preliminary approach, as it provides a computationally efficient estimate that can later be refined using nonlinear implicit analysis for the final table setup.

4.5. Insights from the Design Space Exploration

The iterative simulations conducted for both the 50 kg and 25 kg test specimens provided critical insights that shaped the final shock table design. By systematically refining key parameters such as hammer

material, anvil composition, and impact velocity, it was possible to develop a configuration that meets the required Shock Response Spectrum (SRS) while maintaining efficiency and repeatability.

This section highlights the key takeaways from the design space exploration and how they influenced the final shock table configuration. The decisions made aimed to balance test accuracy, structural integrity, and practical implementation while ensuring compliance with launch vehicle shock requirements.

The selected design consists of a horizontal anvil plate impacted by a dropped hammer, as determined in the conceptual design phase in chapter 2. To ensure consistent and controlled impacts, the hammer is guided along a vertical aluminium tube. A steel cable system, operated by a manually rotated winch mechanism, allows for precise repositioning of the hammer between tests.

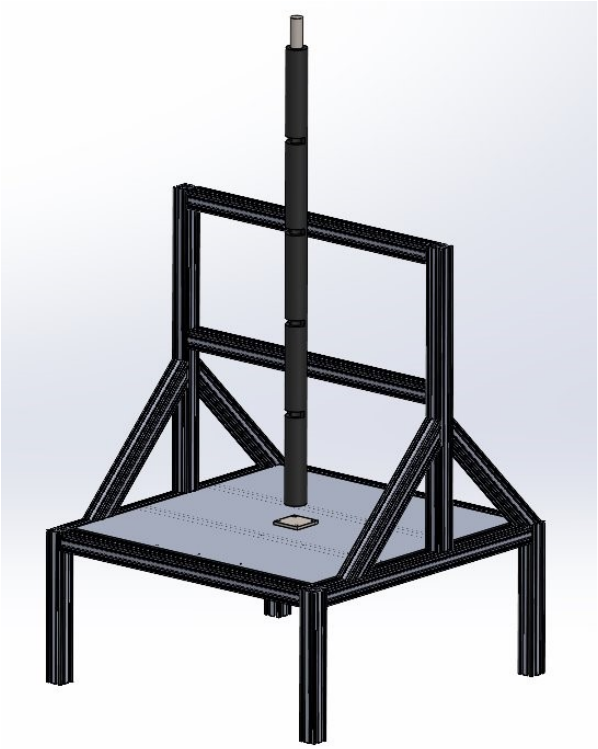

Figure 4.12: Preliminary Final Design of the Shock Table.

The hammer is made of steel, as simulations demonstrated that this material produced the best results in terms of achieving the target SRS. Additionally, simulations showed that increasing the hammer mass was an effective method for tuning the response, particularly at lower frequencies.

To allow for greater flexibility in testing, the final design includes a modular weight system that enables the hammer mass to be adjusted up to six times its baseline mass. This provides a wider range of excitation levels beyond what was tested in simulations, ensuring adaptability for different test requirements.

The hammer will be dropped from a maximum height of 2 meters, allowing for an impact velocity of approximately 6 m/s. This is significantly higher than the 1 m/s velocity used in simulations, ensuring that the system can generate higher excitation levels if needed. The simulation results were treated as a baseline, while the final design allows for a wider range of adjustments to accommodate various test scenarios.

The design space exploration indicated that both steel and aluminium anvils were effective in achieving the desired shock response, depending on the specific frequency range being targeted. To maximise flexibility, the final design considers interchangeable anvil plates, allowing the selection of the most appropriate material based on the specific test requirements.

By integrating insights gained from the simulation process, the preliminary final design of the shock table ensures greater control over impact parameters, providing a tunable test environment capable of meeting a wide range of SRS requirements. The modular nature of the design enables adaptability for future experiments, making it a versatile tool for shock testing applications.

5

Conclusion

This study aimed to develop a shock table using finite element analysis (FEA) to predict shock response spectrum (SRS) levels and evaluate the accuracy of FEA in simulating shock responses. The research focused on understanding how different modelling approaches, solution types, and key parameters affect the predicted shock behaviour.

The first step in studying the accuracy of finite element analysis in predicting shock events, is to conduct a convergence study to understand the effect of mesh size and time step on the response obtained. In the time domain, both mesh size and time step size had a significant effect on the accuracy of the results. Smaller time steps and finer mesh sizes were necessary to achieve convergence, especially for capturing higher-frequency content of the shock response. As expected, larger time steps led to less accurate results, with significant deviations observed in the shock response due to the inability to capture high-frequency behaviour.

When analysing the Shock Response Spectrum (SRS) obtained from the time domain simulations, the mesh size did not have a significant impact on the SRS curve, indicating that finer meshes were not necessary to capture the shock response accurately. However, the time step size had a notable influence on the SRS curve. Larger time steps resulted in an early cutoff of high-frequency content, while smaller time steps allowed for a more accurate representation of the SRS across the entire frequency spectrum.

It is also important to note that when using the Direct Transient solution, the SRS curves from different time step sizes were almost identical up until the cutoff frequency. However, when using the Non-Linear Implicit Transient analysis, slight differences were observed in the SRS curve shapes even before the cutoff, suggesting that smaller time steps may be necessary to obtain accurate results, even if the frequency range of interest is not as large.

A key aspect of this study was the comparison between the Direct Transient and Nonlinear Implicit Transient solution methods. The results revealed distinct differences, especially in the mid-to-high frequency ranges, that highlight the strengths and weaknesses of each approach in modelling shock dynamics.

At low frequencies, below approximately 200 Hz, both methods yield similar results, capturing the first two prominent peaks of the response. However, the peaks obtained from the Direct Transient Analysis appear more spread out, or ‘elongated’, over a wider frequency range compared to the clearer, more defined peaks observed in the Non-linear Implicit Analysis. Additionally, the acceleration levels predicted by the Direct Transient Analysis are slightly higher.

In the mid- and high-frequency ranges, particularly in the 200 Hz–1000 Hz range, the differences between the two methods became more evident. The Nonlinear Implicit Analysis consistently predicted higher acceleration levels and more pronounced oscillations in the SRS, showing clear and defined peaks caused due to the plate’s modes. This is due to the Nonlinear Implicit approach’s ability to accurately model complex contact interactions, wave propagation, and material behaviour during impact,

including realistic simulations of contact separation, wave reflections, and energy dissipation—critical factors for capturing high-frequency dynamics.

In contrast, the Direct Transient method, which uses a simplified approach for contact modelling (via an RBE2 element), resulted in smoother acceleration responses. This simplification under-represented high-frequency components in the SRS, particularly at the higher end of the frequency spectrum. The Direct Transient method does not model detachment or non-linear wave propagation, meaning that energy dissipation and wave reflections are not fully captured, leading to less accurate shock responses at higher frequencies.

This key difference in the handling of contact interactions and wave effects suggests that while the Direct Transient method is computationally more efficient and suitable for basic simulations, the Non-linear Implicit Transient approach provides a more realistic and accurate representation of complex shock events, especially in scenarios involving high-frequency shock responses, non-linear material behaviour, and dynamic contact interactions.

Overall, the results suggest that for low-frequency shock analysis, the Direct Transient Analysis could be a computationally efficient solution that captures the overall behaviour of the structure without too much detail. However, for accurate predictions of high-frequency behaviour and real-world shock dynamics, the Nonlinear Implicit Transient Analysis is the preferred solution due to its ability to model the complexities of material and contact behaviour.

The inclusion of additional structural elements, such as the anvil and the test mass, also had a significant effect on the response obtained in the simulations. The effect of model detail was particularly noticeable in both the Direct Transient and Nonlinear Implicit analyses, with more detailed models showing a more accurate and complex shock response.

When considering the impact of adding the Anvil, the results showed higher acceleration values throughout the frequency range of interest in the Direct Transient Analysis, indicating that the Anvil enhances shock energy transmission and introduces additional structural interactions. However, in the Nonlinear Implicit Analysis, this increase in acceleration was only observed in the lower to mid-frequency ranges. At higher frequencies, the Nonlinear Implicit model showed a significant dampening of the response. This dampening effect can be attributed to the more realistic simulation of non-linear contact interactions, such as contact separation and wave dissipation, which are more accurately captured in the Nonlinear Implicit model.

Similarly, the Test Mass had a dampening effect on the shock response, particularly at higher frequencies. This dampening effect was more pronounced in the Nonlinear Implicit Analysis, which is better at capturing energy dissipation mechanisms, resulting in a more pronounced reduction of peak accelerations at high frequencies. Additionally, the test specimen mass also led to a shift to the left in the peaks of the response.

The sensitivity of the shock response to variations in key parameters was a crucial aspect of this study. The analysis revealed that changes to certain parameters had more significant impacts on specific regions of the SRS. These insights helped identify the most critical parameters for adjusting the shock table setup to achieve a balanced shock response across the entire frequency spectrum.

Both the Direct Transient and Non-Linear Implicit methods were effective in capturing the basic trends of shock response. For impact velocity, both methods predicted a uniform rise in the SRS curve as the velocity increased, which indicates their capability to capture the proportional increase in shock amplitude due to higher velocity. When analysing the effect of anvil material, the analysis revealed that harder materials, such as stainless steel, resulted in higher peak accelerations, particularly at higher frequencies. Similarly, changes to hammer mass had a significant impact on the shock response, with an increase in hammer mass leading to stronger shock responses, particularly at lower frequencies. Lastly, both solution types predicted that increasing test specimen mass resulted in a downward shift in the SRS curve, particularly at higher frequencies. As such, both analysis methods were considered suitable for these types of parameter studies.

As the ultimate goal of any shock testing facility is to replicate the required SRS levels provided by launch vehicle specifications, a series of iterative simulations were conducted to match the obtained

SRS values with those provided by SpaceX for the Falcon 9 launch vehicle. This process was approached as a design space exploration to determine the optimal shock table setup, influencing decisions for the final design. The Nonlinear Implicit Transient solution was used on the most detailed model, including the anvil and test mass, to ensure accuracy in the results.

The comparison of results for two test specimens, one with a 50 kg mass and the other with a 25 kg mass, highlighted the influence of specimen mass on shock response. The 50 kg specimen presented more challenges in achieving a close match to the target SRS, especially in the low-frequency range, where discrepancies were more pronounced. These discrepancies required more adjustments to the shock table parameters to ensure the simulated response aligned with the target. In contrast, the 25 kg test specimen was easier to align with the target SRS due to its lighter mass, requiring fewer modifications to the shock table setup.

5.1. Future Work

While this study has provided valuable insights into the development and simulation of shock tables using finite element analysis (FEA), several areas remain open for further exploration. Future work can focus on refining the current methodologies, expanding the scope of the study, and exploring new avenues to improve shock testing accuracy and efficiency.

Although this study focused on comparing the Direct Transient and Nonlinear Implicit Transient methods, it would be beneficial to explore other solution techniques for shock event prediction. For example, one of the main drawbacks of explicit methods is their conditional stability, meaning that very small time steps are required to ensure convergence, which can lead to an increase in computational time. However, due to the short duration of shock, small time steps are already a requirement for this type of analysis. Therefore, the explicit method may provide a more computationally efficient solution compared to implicit methods for shock events, as each response at the current time step is calculated based on the system's state, without requiring iterations, which can be a time-consuming process in implicit methods. Thus, explicit methods can be a more efficient option when dealing with short-duration, high-frequency shock events.

Additionally, further refinement of the simulation models by incorporating more structural detail would enhance the accuracy of the predictions. For instance, modelling the entire shock table structure, rather than focusing solely on the main components directly involved in the shock event, could offer a more comprehensive view of the system's response. This could help in understanding how less directly involved parts of the shock table contribute to the overall behaviour, particularly in complex shock scenarios.

Lastly, the experimental validation of the predicted results should be a key focus of future work. Performing physical shock testing, including the use of accelerometers and SRS measurements on actual shock tables, would allow for a direct comparison with the simulation results. This step is essential for identifying discrepancies between simulated and experimental data, which would provide valuable feedback for refining the simulation models and improving their predictive accuracy.

References

[1] C. D. Risner, “Development of cal poly’s shock table,” 2016. DOI: 10.15368/theses.2016.151.

[2] S. e. a. Aitzaid, *ECSS-E-HB-32-25A: Mechanical shock design and verification handbook*, 1st ed. ESA Requirements and Standards Division, 2015.

[3] J. Martin, “Development of a shock test facility for qualification of space equipment,” 2012.

[4] C. M. Harris and A. G. Piersol, “Harris’ shock and vibration handbook,” 1976.

[5] S. E. T. Corp., *Rideshare payload user’s guide*, Version 10, Accessed: 29 January 2025, Sep. 2024. [Online]. Available: https://www.spacex.com/rideshare/index.html.

[6] E. S. A. (ESA), *ECSS-E-ST-10-03C: Space Engineering Testing*, 2nd ed. ESA Requirements and Standards Division, 2012.

[7] N. Aeronautics and S. A. (NASA), *NASA-STD-7003A: Pyroshock Test Criteria*, 2nd ed. NASA, 2011.

[8] N. T. Davie and V. I. Bateman, “Pyroshock simulation for satellite components using a tunable resonant fixture - phase 2,” *Technical Report*, 1997. DOI: 10.2172/469143.

[9] J. Lee, C. Chia, and C. Kong, “Review of pyroshock wave measurement and simulation for space systems,” *Measurement*, vol. 45, no. 4, pp. 631–642, 2012. DOI: 10.1016/j.measurement.2011.12.011.

[10] J. Wang, Y. Li, and Y. Wen, “Experimental study on the generated pyroshock level under different amount of explosive,” *Vibroengineering PROCEDIA*, vol. 20, pp. 191–195, 2018. DOI: 10.21595/vp.2018.20198. [Online]. Available: https://doi.org/10.21595/vp.2018.20198.

[11] T. J. Dwyer and D. S. Moul, “Pyro shock simulation: Experience with the mips simulator,” 1988.

[12] G. Schweickert, “The dornier shock table - a new facility for shock testing of components,” *Environmental Testing for Space Programs*, 1997.

[13] A. Almesmari, F. Jarrar, F. Almaskari, P. Marpu, N. Shukoor, and J. Govindan, “Development of a metal-to-metal mid-field shock test procedure for nanosatellites,” *IEEE Journal on Miniaturized Air and Space Systems*, 2020. DOI: 10.1109/jmass.2020.3005190.

[14] S.-J. Lee, D.-H. Hwang, and J.-H. Han, “Development of pyroshock simulator for shock propagation test,” *Shock and Vibration*, vol. 2018, pp. 1–13, 2018. DOI: 10.1155/2018/9753793.

[15] J. G. Jang, J.-K. Jang, and J.-R. Lee, “Nondestructive prediction of point source pyroshock response spectra based on experimental conditioning of laser-induced shocks,” *Optics and Laser Technology*, vol. 61, pp. 24–33, 2014. DOI: 10.1016/j.optlastec.2014.02.005.

[16] A. García-Pérez, F. Sorribes-Palmer, G. Alonso, and A. Ravanbakhsh, “Overview and application of fem methods for shock analysis in space instruments,” *Aerospace Science and Technology*, vol. 80, pp. 572–586, 2018. DOI: 10.1016/j.ast.2018.07.035.

[17] B.-S. Kim and J. Lee, “Development of impact test device for pyroshock simulation using impact analysis,” *Aerospace*, vol. 9, p. 407, 2022. DOI: 10.3390/aerospace9080407.

[18] T. Yalçinkaya and B. Gürsoy, “Numerical validation of a pyroshock test system and application to qualification tests,” *Aerospace*, vol. 9, p. 400, 2022. DOI: 10.3390/aerospace9080400.

[19] X. Wang, Z. Qin, J. Ding, and F. Chu, “Finite element modeling and pyroshock response analysis of separation nuts,” *Aerospace Science and Technology*, vol. 68, pp. 380–390, 2017.

[20] D. Hipparkar, M. S. Baghel, and S. Chandel, “Characterization of acceleration shock pulse by finite element analysis and validation by shock testing on heavy mass test objects for defense applications,” *International Journal of Engineering Trends and Technology*, vol. 71, pp. 23–32, 2023.

[21] L. Viale, A. P. Daga, L. Garibaldi, and A. Fasana, “Numerical modeling of a pyroshock test plate for qualification of space equipment,” Springer International Publishing, 2023, pp. 990–999, ISBN: 978-3-031-07321-2. DOI: 10.1007/978-3-031-07322-9_100.

[22] L. Viale, A. P. Daga, A. Fasana, and L. Garibaldi, “On pyroshock tests for aerospace equipment qualification: A comprehensive parametric model for the simulation and the design of pyroshock test facilities,” *International Journal of Impact Engineering*, vol. 180, p. 104 697, 2023. DOI: 10.1016/j.ijimpeng.2023.104697.

[23] NASA and G. Shea, *NASA Systems Engineering Handbook*. 2007. [Online]. Available: https://repository.exst.jaxa.jp/dspace/handle/a-is/256897.

[24] T. Saaty, L. Vargas, and S. Cahyono, *The Analytic Hierarchy Process*. Springer, 2022, ISBN: 978-1-4614-3597-6.

[25] M. S. Corporation, *MSC Nastran 2012 Quick Reference Guide*. MSC Software, 2012, Available from MSC Software documentation.

[26] S. D. I. Software, *NX Nastran Advanced Dynamics User’s Guide*. Siemens PLM Software, 2020, Accessed from official Siemens documentation.

[27] MSC Software Corporation, *MSC Nastran 2020 Reference Guide*, Available from MSC Software with licensed access, Hexagon, 2020.

[28] T. Irvine, *Shock response spectrum*, MATLAB Central File Exchange, Retrieved January 29, 2025, 2025. [Online]. Available: https://www.mathworks.com/matlabcentral/fileexchange/7398-shock-response-spectrum.

[29] J. E. Alexander, “Shock response spectrum – a primer,” in *IMAC-XXVII, the 27th International Modal Analysis Conference*, Society for Experimental Mechanics, Orlando, FL, Feb. 2009.

[30] D. O. Smallwood, “Improved recursive formula for calculating shock response spectra,” *Shock and Vibration Bulletin*, no. 51, May 1981. [Online]. Available: https://www.osti.gov/biblio/5181963.

A

Shock Response Spectrum

The Shock Response Spectrum (SRS) is a widely used tool for characterizing and analysing the effects of shock loading on mechanical systems. It provides a frequency-domain representation of the peak responses of a series of Single Degree of Freedom (SDOF) oscillators subjected to a given acceleration time history [2]. This approach allows engineers to assess how different structural components will respond to transient shock events, making it particularly useful for aerospace applications where shock loads are a critical design consideration.

The SRS is derived by passing the input acceleration time history through an array of damped SDOF systems, each with a unique natural frequency [29]. The response of each oscillator is computed using:

$$m\ddot{x} + c\dot{x} + kx = F(t) \tag{A.1}$$

where:

- m is the mass of the oscillator,
- c is the damping coefficient,
- k is the stiffness,
- x is the displacement, and
- $F(t)$ is the applied force, derived from the input acceleration.

For each oscillator, the maximum absolute acceleration response is recorded. Plotting these peak responses against their respective frequencies results in the SRS curve. Figure A.1 presents the process just described for the calculation of the SRS curve.

Damping significantly influences the computed SRS. Most SRS calculations assume a damping ratio of 5%, which is a typical value for aerospace structures [2]. Higher damping levels result in lower response amplitudes, particularly at resonance, while lower damping values lead to sharper peaks in the spectrum.

To efficiently compute the SRS from a simulated acceleration time history, the Smallwood recursive algorithm is used [30]. This method provides a computationally efficient way to determine the peak response of each SDOF system without requiring direct numerical integration.

The Smallwood method reformulates the differential equation into a discrete-time recursive relation, allowing the response to be computed iteratively without solving the full equation at every time step [30]. The acceleration response at each time step is obtained using the general recursive form:

$$\ddot{x}n = b_0\ddot{x}m + b_1\ddot{x}m - 1 + b_2\ddot{x}m - 2 - a_1\ddot{x}n - 1 - a_2\ddot{x}n - 2 \tag{A.2}$$

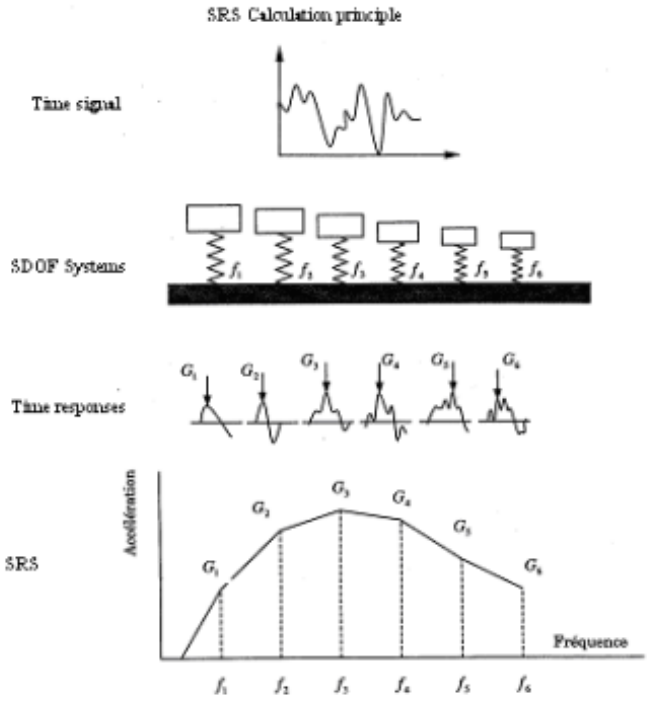

Figure A.1: Shock Response Spectrum Principle [2]

where $\ddot{x}_n$ represents the acceleration response at the current time step, and the coefficients a_1, a_2, b_1, b_2 and b_3 depend on the natural frequency, damping ratio, and time step size. These coefficients ensure that the solution accounts for the damping effects while maintaining numerical stability.

B

Gantt Chart

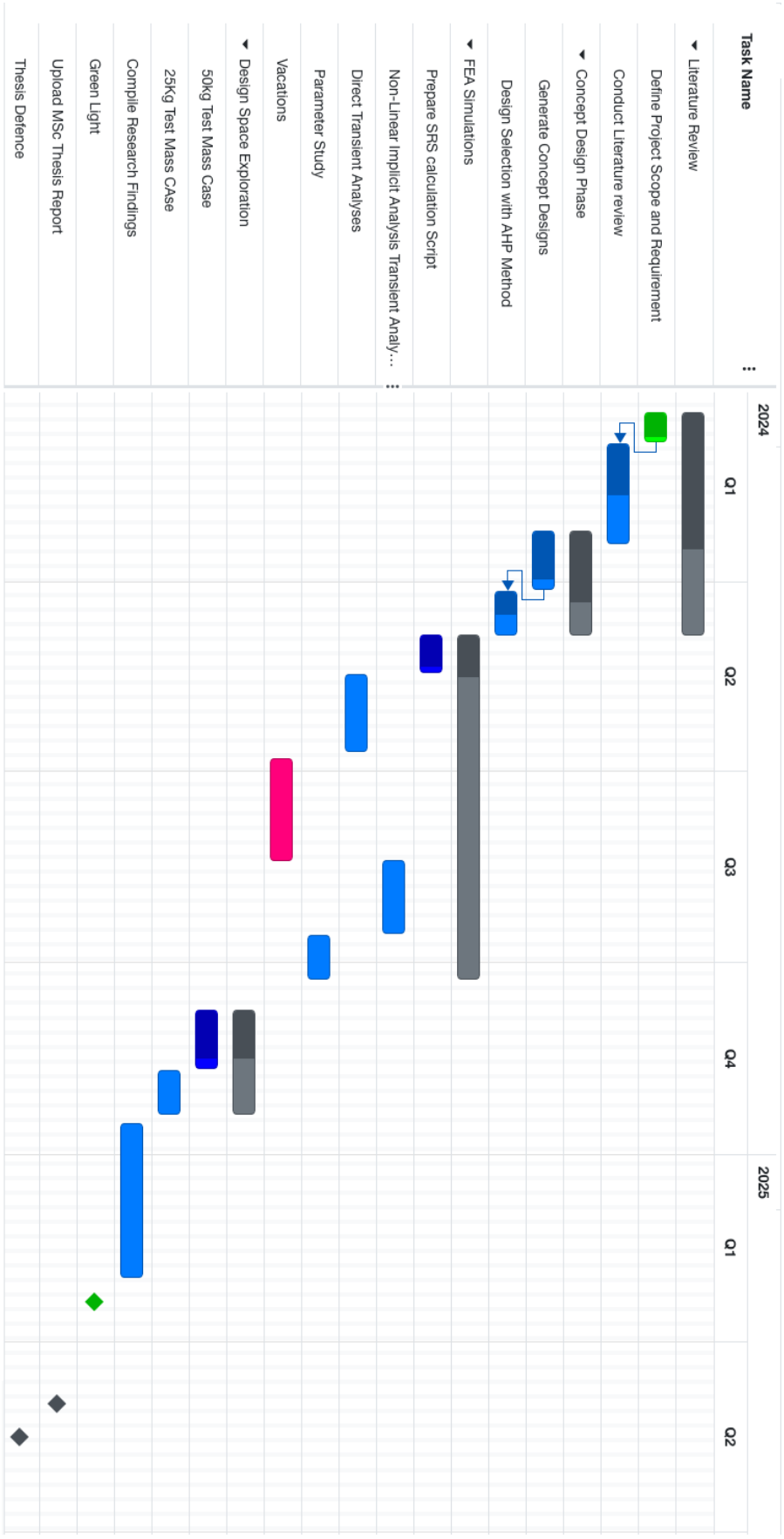
Task Name
2024
Q1
Q2
Q3
Q4
2025
Q1
Q2
Literature Review
Define Project Scope and Requirement
Conduct Literature review
Concept Design Phase
Generate Concept Designs
Design Selection with AHP Method
FEA Simulations
Prepare SRS calculation Script
Non-Linear Implicit Analysis Transient Analy...
Direct Transient Analyses
Parameter Study
Vacations
Design Space Exploration
50kg Test Mass Case
25Kg Test Mass CAse
Compile Research Findings
Green Light
Upload MSc Thesis Report
Thesis Defence